SECURITY CLASSIFICATION OF THIS PAGE

REPORT DOCUMENTATION PAGE

1a REPORT SECURITY CLASSIFICATION UNCLASSIFIED	1b RESTRICTIVE MARKINGS
2a SECURITY CLASSIFICATION AUTHORITY	3 DISTRIBUTION / AVAILABILITY OF REPORT Approved for public release; distribution unlimited.
2b DECLASSIFICATION / DOWNGRADING SCHEDULE	
4 PERFORMING ORGANIZATION REPORT NUMBER(S) NRL Memorandum Report 5610	5. MONITORING ORGANIZATION REPORT NUMBER(S)
6a. NAME OF PERFORMING ORGANIZATION Naval Research Laboratory 6b OFFICE SYMBOL (*If applicable*) Code 5841	7a. NAME OF MONITORING ORGANIZATION Office of Naval Research
6c. ADDRESS (*City, State, and ZIP Code*) Washington, DC 20375-5000	7b. ADDRESS (*City, State, and ZIP Code*) Arlington, VA 22217
8a. NAME OF FUNDING / SPONSORING ORGANIZATION Office of Naval Research 8b. OFFICE SYMBOL (*If applicable*)	9. PROCUREMENT INSTRUMENT IDENTIFICATION NUMBER
8c. ADDRESS (*City, State, and ZIP Code*) Arlington, VA 22217	10. SOURCE OF FUNDING NUMBERS PROGRAM ELEMENT NO. 61153N; PROJECT NO.; TASK NO. RR023-01041; WORK UNIT ACCESSION NO. DN380-021
11 TITLE (*Include Security Classification*) Laboratory Studies of Steep and Breaking Deep Water Waves in a Convergent Channel	
12 PERSONAL AUTHOR(S) Ramberg, S.E., Barber, M.E. and Griffin, O.M.	
13a. TYPE OF REPORT Interim 13b. TIME COVERED FROM 8/83 TO 5/85	14. DATE OF REPORT (*Year, Month, Day*) 1985 August 21 15. PAGE COUNT 47
16 SUPPLEMENTARY NOTATION	
17 COSATI CODES FIELD / GROUP / SUB-GROUP	18. SUBJECT TERMS (*Continue on reverse if necessary and identify by block number*) Wave breaking; Ocean waves; Ocean engineering

19 ABSTRACT (*Continue on reverse if necessary and identify by block number*)

There are many causes for the breaking of ocean waves. These include the relative motion between the water and, say, a ship in the seaway or a cylindrical obstacle in a wavefield; wind blowing over the water; superposition of and nonlinear interactions between wave components; concentration of wave energy by refraction; and the shoaling of waves. These various causes result in two predominant types of breaking waves; the plunging breaker, in which the wave crest curls forward and plunges into the slope of the wave at some distance away from the crest; and spilling breakers, in which the broken region tends to develop more gently from an instability at the crest and often forms a quasi-steady whitecap on the forward face of the wave. Spilling and plunging breakers are most commonly found in deep water.

The present experiments were conducted to study the evolution of steep and breaking deep water waves. The waves were made to steepen by a convergent section which was installed in NRL's 30m long wave channel. These and other recent experiments have demonstrated that a criterion for the onset of breaking for deep water waves

(Continues)

20 DISTRIBUTION / AVAILABILITY OF ABSTRACT ☒ UNCLASSIFIED/UNLIMITED ☐ SAME AS RPT. ☐ DTIC USERS	21. ABSTRACT SECURITY CLASSIFICATION UNCLASSIFIED
22a NAME OF RESPONSIBLE INDIVIDUAL Owen M. Griffin	22b. TELEPHONE (*Include Area Code*) (202) 767-2904 22c. OFFICE SYMBOL Code 5841

DD FORM 1473, 84 MAR 83 APR edition may be used until exhausted.
All other editions are obsolete.

SECURITY CLASSIFICATION OF THIS PAGE

19. ABSTRACT (Continued)

can be simply stated in terms of the wave steepness at breaking. This criterion states that the wave steepness at the onset of breaking is given by $H/L_* \simeq 0.11$, where H is the wave height and L_* is the Stokes limiting wavelength (Mitchell, 1893). On the evidence available thus far the simple steepness criterion applies equally well to spilling and plunging breakers. Criteria such as this can be readily used to predict the frequency of occurrence of breaking for deep water waves (Nath and Ramsey, 1976; Ochi and Tsai, 1983).

There are more complex questions relating to energy losses in breaking and related topics which cannot be addressed so simply. From the results of the present experiments it appears that the potential energy loss rates of plunging breakers are twice those of spilling breakers in deep water. Moreover, the potential energy losses in breaking did not significantly alter the total mean drift and return flows in the channel. Most of the energy lost goes into the production of turbulence and into air entrainment in the breaking region.

NRL Memorandum Report 5610

Laboratory Studies of Steep and Breaking Deep Water Waves in a Convergent Channel

S. E. RAMBERG, M. E. BARBER AND O. M. GRIFFIN

Fluid Dynamics Branch
Marine Technology Division

August 21, 1985

NAVAL RESEARCH LABORATORY
Washington, D.C.

CONTENTS

LABORATORY STUDIES OF STEEP AND BREAKING DEEP WATER WAVES IN A CONVERGENT CHANNEL

1. INTRODUCTION AND BACKGROUND

For more than a century hydrodynamicists have been exploring the nonlinear behavior of ocean surface waves, with one special goal being a rationale for and a description of the catastrophic nonlinearity commonly known as wave breaking. The breaking of ocean waves, either occuring naturally in ambient seas or forced as in shoaling waters and in interactions with man-made structures, is a common observation and an important element of many oceanographic, coastal and ocean engineering problems. Wave breaking is also an important consideration in surface ship hydrodynamics. The wave resistance of a ship is influenced by the breaking of the ship's bow wave. In addition, the wake energy balance and the ensuing white water production must account for wave breaking.

Several significant advances toward an understanding of wave breaking have been made in recent years. These include the experimental characterization of instability mechanisms which can lead to wave breaking, mathematical models for these instability mechanisms, and numerical simulations of wave overturning and incipient breaking. Empirical and semi-empirical models have been proposed to describe the breaking of steady waves generated by the relative motion between the water and submerged bodies or to describe the later stages of spilling breakers, tidal bores, and hydraulic jumps. Much is still unknown, however, including such simple information as a criterion for the onset of breaking.

Manuscript approved April 15, 1985.

1.1 Wave Breaking in Deep Water Wave breaking in deep water has drawn increasing attention from numerous investigators with concerns ranging from the improvement of ship performance and safety, or the prediction of forces on marine structures, to a better understanding of the fundamentals of the nonlinear surface wave phenomena which lead to wave breaking. The causes of wave breaking are varied and often are reflected in the manner in which a wave breaks; from gentle spilling at the crest to sometimes spectacular curling and plunging of the forward face of the wave. In deep water, the most common breakers are spilling, and, in the presence of sufficient wind, white-capping. Studies of wave breaking generally focus first upon the conditions which correspond to the onset of breaking. This is often followed by the examination of particular wave characteristics of importance to the application at hand.

Recent studies of deep water breaking have largely dealt with the growth of subharmonic instabilities of steep, initially regular waves that lead to two and three-dimensional spilling breakers. A summary and discussion of this material is given by Griffin (1984). In these recent studies a uniform wave train of initial steepness $s_o = a_o k_o$ evolves to breaking. Here a is the wave amplitude, $k = 2\pi/L$ is the wavenumber based on wavelength L and the subscript is used to denote initial values. On comparison of the experiments performed by Kjeldson et al (1978,1979,1980), Melville (1982) and Su et al (1982,1984); and with the analyses of Longuet-Higgins (1978b), Cokelet (1979), Vinje and Brevig (1981), and McLean et al (1981) there is generally good agreement that the following processes take place. For $0.15 < s_o \leq 0.25$ the evolution to breaking is essentially two-dimensional with the instabilities corresponding to the most unstable modes predicted by Longuet-Higgins (1978b) versus the classical Benjamin-Feir analysis (1967). For $0.25 \leq s_o < 0.35$ two dimensional disturbances quickly give way to three-dimensional crescent-shaped breakers which ultimately are transformed into a long-crested wave system with lower steepnesses and frequencies.

The profiles of the breaking waves photographed by Melville at $ak < 0.3$ show general agreement with the numerical solutions of Longuet-Higgins and Cokelet and with those of Vinje and Brevig (1981), and can be used to interpret not only the wave motion before breaking but also the wave motion in the breaking region.

One of the dismaying features of these results is that the manner of breaking is not specified. In fact, the numerical simulations generally predict plunging breakers while the experiments produce spilling breakers with only occasional mildly plunging breakers. To classify the breaking waves Kjeldsen et al introduced several non-dimensional wave steepness parameters. The most important was thought to be the so-called "crest front steepness", or

$$\varepsilon = \frac{a'}{\lambda'} , \qquad (1.1.1)$$

where a' is the vertical distance from the mean water level to the wave crest and λ' is the horizontal distance from the zero upcross point on the wave to the wave crest. The crest front steepness was considered to be more representative of the asymmetric profile of an overturning wave, as compared to the more usual wave steepness, ak. Typical values of ε for the breaking wave experiments of Kjeldsen et al were in the range

$$0.32 < \varepsilon < 0.78.$$

The highest values of ε corresponded to plunging breakers, while spilling breakers were of lower steepnesses. In the present study we define a symmetry parameter, α, to be one-half of the wavelength divided by the horizontal distance from the crest to the preceding trough.

Another difficulty with the existing instability calculations is the somewhat ambiguous nature of the criterion for wave breaking. Waves with identical initial steepnesses in the range $0.10 \leq s_o \leq 0.15$ may or may not break, and in the range $0.15 \leq s_o \leq 0.25$ the eventual location and form of breaking can vary significantly, depending upon the initial value of $s_o = a_o k_o$. These variations are expected on the basis of Longuet-Higgins' analysis, and this is one reason why his contribution is so impressive. It cannot, however, address the general problem of the breaking of ocean waves

where the time scales for the growth of weak instabilities may exceed the characteristic times for stationarity and almost certainly exceeds the time scales for interactions among various spectral components which may be travelling in different directions. The present experiments were conducted to address this issue through studies of the breaking of waves which are growing under an external influence.

1.2 Previous Convergent Channel Experiments Van Dorn and Pazan (1975) conducted a systematic laboratory study of deep water wave breaking. A convergent section was installed inside a wave channel to increase the steepness of the wave train. The convergence of the channel was 1:10 over a length of 19m (62.3 ft) followed by a narrow uniform section 0.5m (1.6 ft) in length by 0.52m (1.7 ft) in width. The water depth in the channel was varied with the wave period in order to insure the generation of deep water waves.

When the local wave steepness was less than ak = 0.3 the wave profiles remained approximately symmetric and Stokes' fifth-order wave theory gave a good description of the wave properties. This was called the "young" wave regime. For wave steepnesses between $0.3 < ak < 0.38$ the wave profiles became increasingly asymmetric with a steep forward face. Most of the change in the profile was confined to that portion of the wave above the still water level. The rate of increase of potential energy density along the channel before breaking was inversely proportional to the channel width because the experiments were done with a 'burst' of waves before a mean flow could be established. Thus the energy flux was simply conserved. This was called the "pre-breaking" regime.

Wave breaking occurred spontaneously when $0.38 < ak < 0.44$. The forward face of the wave became nearly vertical and a jet of water issued from the forward face just below the crest. This appears to be similar in character to the overturning process which precedes the plunging of a breaker. The maximum jet velocity approached the limiting value $c_{L/M} = 1.2\ g/\omega$ for Stokes waves of maximum height. This was called the "breaking"

regime by Van Dorn and Pazan. Table 1 summarizes the characteristics of the three wave regimes.

Table 1

DEEP WATER WAVE BREAKING IN A CONVERGENT CHANNEL+

Wave Steepness	Wave Characteristics
$ak<0.3$	"Young" waves-symmetric about the crest; Stokes' fifth-order theory applies.
$0.3<ak<0.38$	"Pre-breaking" waves-asymmetric waves with steep forward faces; streamlines distorted.
$0.38<ak<0.44$	"Breaking" waves-vertical forward face of the wave; overturning and plunging of the waves.

+From Van Dorn and Pazan (1975).

The wave steepnesses at breaking in Table 1 are higher than those observed by Melville (1982), Su et al (1982, 1984), and by Duncan (1983). The convergent walls of the channel together with the transient nature of the experiment may have led to breaking before the instability mechanisms naturally could produce a breaker as discussed in the previous section.

The breaking intensity, defined by Van Dorn and Pazan in terms of the potential energy loss rate, was correlated with the potential energy

increase before breaking. The energy dissipation due to breaking (normalized by the product of wave frequency and mean wave energy) was approximately a linear function of the growth rate of the waves. This led Van Dorn and Pazan to suggest that history effects were likely to be important in any deterministic theory for wave breaking. In addition it was found that the energy losses after wave breaking were in equilibrium with the energy input due to the convergent channel. These findings are not in complete agreement with the present results.

More recently Kjeldsen and Myrhaug (1979,1981) conducted experiments in a wave channel which contained a convergent section with a slope of 1:23. The purpose of the experiments was to study the impact pressures due to breaking waves acting on submerged plates. In all cases the waves were deep water spilling breakers. Shock pressures were observed to occur for both spilling breakers and for steep non-breaking waves. The magnitudes of the shock peaks were a function of the ratio ε/s of the crest front steepness ε and the total steepness s. No deep water wave breaking criteria were derived from these experiments.

1.3 Conservation Relations The conservation of mass and energy fluxes in a convergent laboratory channel is complicated both by the convergence and by the finite length of the channel. Wave energy is reflected and the net mass flow through a vertical plane is constrained to be zero at any location in the channel. The latter condition leads to the simple relation

$$\bar{U} = - \dot{m} w d \qquad (1.3.1)$$

by assuming that the rate of convergence is small enough for a slowly varying, nearly one-dimensional flow approximation. Here $\dot{m}$ is the local wave-induced mass flux, $\bar{U}$ is the local depth-averaged mean return current and (wd) is the mean local area given by the product of local width w and mean depth d. The experiments by Van Dorn and Pazan attempted to avoid this complication by generating a 'burst' of waves, and then taking data after the initial wave transients, but before the finite channel length could exert any influence. That approach raises questions of stationarity for the

interim steady-state which is assumed to exist. For our experiments it was observed that a steady-state was often difficult to reach even for constant input parameters. This is discussed later in some detail.

For the convergent, finite length channel with steady generation of waves we assume that the energy flux is governed by

$$\frac{\partial}{\partial x_i}\left[\left(U_i + C_{gi}\right)E\right] + S_{ij}\frac{\partial U}{\partial x_i} = 0 \qquad (1.3.2)$$

where U_i is the depth-averaged mean flow in the ith direction, C_{gi} is the group velocity, E is the total wave energy, and S_{ij} is the radiation stress. This equation stems from an energy balance for the fluctuating motions (Phillips, 1977) where the flow is steady in the mean and dissipation is neglected. We further assume that the flow in a slowly convergent channel is effectively one-dimensional and then apply Equation (1.3.2) to a differential element of the convergent channel as shown below.

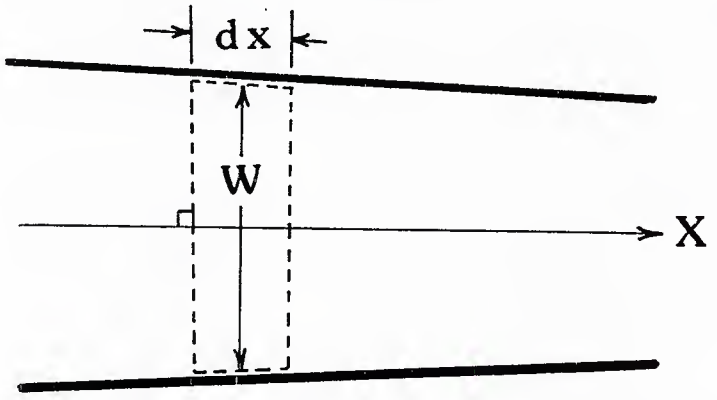

Integration and application of Green's theorem yields the relation

$$\frac{d}{dx}\left[Ew(U+C/2)\right] + w\,\frac{E}{2}\,\frac{dU}{dx} = 0 \qquad (1.3.3)$$

where the substitutions $S_{11} = E/2$ and $C_g = C/2$ have been made for deep water conditions. The channel width w is a slowly varying function of x. If the mean flow U is ignored or absent the conservation requirement reduces to

$$\frac{d}{dx}\left[Ew\ C/2\right] = 0 \qquad (1.3.4)$$

or

$$CEw = Fw = \text{constant} \qquad (1.3.5)$$

where $F = CE$ is the energy flux. This is the conservation equation employed by Van Dorn and Pazan under the assumption that their data were obtained before a mean flow could be established. This is a reasonable assumption as stated, but it overlooks the influence of time dependent $\frac{\partial}{\partial t}$ terms dropped earlier. These may become significant locally and therefore may markedly influence any transitional events such as wave breaking. On the basis of this simple relation Van Dorn and Pazan introduced a growth rate $G = -L_*\left(\frac{dw}{dx}\right)/w$ to express the amplification within their channel. Here $L_* = 1.2gT^2/2\pi$ is the Stokes limiting wavelength (Michell, 1893), which has the advantage of simplicity while approximating the actual wavelength near breaking. We will retain the use of L_* and G in the presentation of our results, but the physical significance of G is reduced to a non-dimensional channel convergence. It is useful in that sense because it describes the rate of convergence experienced by a wave in the distance of one wavelength L_*.

The full conservation relation in Equation (1.3.3) can be integrated exactly to give

$$Ew\ (U+C/2) = \text{constant} \qquad (1.3.6)$$

for the conserved quantity in our wave channel.

2. THE WAVE CHANNEL FACILITY AND EXPERIMENTAL METHODS

2.1 The Wave Channel System The facility used in the experiments is the wave channel described by Griffin and Plant (1982). The channel is 30m long and 1.3m wide with about 1.0m of mean water depth. A section of side of the channel is constructed of clear acrylic panels. Several additional viewing locations are available through the channel floor and through the opposite

wall. The waves are generated at one end by a bulkhead wavemaker powered by a variable speed D.C. motor. Waves are absorbed at the downstream end of the channel by a porous sloping beach covered with layers of packing material.

For the present experiments a convergent section was constructed as shown schematically in the bottom of Figure 1. During the initial testing of the facility the wavemaker bulkhead remained normal to the original walls and the uniform test section was terminated just short of the beach. The premise for this arrangement was that the straight channel wall represented a plane of symmetry to the wave system. Large reflections and crosswaves were observed with this arrangement and these were greatly reduced by canting the wavemaker surface normal to the converent channel centerline and by extending the uniform section to the wave absorbing beach at the end of the channel. Although this greatly reduced the crosswaves and reflections, measurable levels of both remained throughout the experiments. Their influences upon the results are discussed in later sections.

2.2 Waveheight Measurements The water surface elevations in the channel were obtained from two capacitance-type wave probes mounted on an overhead carriage that moved under computer control. The carriage paused at twenty two locations in addition to the start and stop positions. At each position eight consecutive wave cycles of data were recorded and digitized for both probes. Several runs were conducted without carriage movement to indicate the stationarity of the experiment. The sampling rate was fixed at twenty five points per wave period in relationship to the wavemaker motion signal. The wave probes were statically calibrated before and after each run. The results obtained from one probe indicated an electronic error which was corrected in the data processing after some careful dynamic calibrations of the offending device.

The experiments were conducted at seven wave periods and at a variety of wavemaker strokes as listed in the Appendix. The strokes were chosen at the outset of each series to obtain data for wave amplification without breaking. The wavemaker stroke was then gradually increased to yield

breakers at various locations in the channel. Figure 1 contains a plot of the averaged waveheight $\bar{H}(x)$ along the channel divided by the wavemaker stroke S for a typical moving carriage run. Here $\bar{H} = \frac{1}{8} \sum_{i=1}^{8} H(x)$ which is the average of eight consecutive crest-to-trough measurements at each probe location. The dashed line in the figure represents the wave amplification predicted from the simple conservation of energy ($H(x) \sim \text{width}^{-1/2}$) and linear wavemaker theory.

A number of important features of the experiments and the present analysis are illustrated in this figure. The first is the occurrence of a standing wave pattern owing to partial reflection of the waves from the end of the channel. The magnitude of the reflected wave component is generally five percent or less. A second effect is demonstrated by the discrepancy between the wave amplitudes recorded by the two probes in Figure 1 over the same section of the channel near x = 29 ft (8.8m). This discrepancy stems from temporal modulations of the waves at a subharmonic of the wave frequency and from slowly varying conditions in the channel. The third effect is a measured wave amplification which is generally less than the theoretical prediction. This behavior was observed in all cases to varying degrees and is due to the combination of finite amplitude waves and a steady-state reverse flow in the closed channel as discussed in Section 1.3. A fourth effect, due to wave breaking, is the decay of the wave amplitude along the channel following the onset of breaking which usually occurs near the end of the convergent section. This decay is a direct measure of the energy lost in breaking. The fifth effect is the presence of crosswaves which are shown rather dramatically in Figure 2a near x = 22 ft (7m). The probes traversed the channel along the straight wall and therefore were very sensitive to crosswaves. The maximum crosswave occurred at a channel width equal to one-half of the local wavelength and then decayed rapidly on either side of the maximum as indicated in the figure. In the other runs the crosswave maximum was beyond the measurement interval.

Not only do these effects occur together but also they influence one another. The location of the wave breaking in the channel was influenced by

both the temporal variations and the spatial modulations due to the reflections. These in turn are influenced by changes in the wave breaking. In many cases a steady-state was never reached. Conditions could be chosen so that the waves would, over a period of 20 to 30 minutes, evolve from an incipient breaking condition to fully breaking and back again. We attempted to record the data in these instances during the periods when breaking waves existed in the channel. Exceptions to this behavior were noted for the subsequent processing of data.

The processing of the data included removal of the spatial variations due to reflections and due to crosswaves in order to obtain smoothed functions of $\bar{H}(x)$ for comparison with various predictions and theories. These results for all runs are plotted in Figure 2. Short period modulations of $H(x)$ were largely removed through the use of $\bar{H}(x)$, whereas longer term variations remained in the data and could only be accounted for qualitatively in the interpretation of results.

2.3 Fluid Velocity Measurements The primary velocities of interest here are the mean flow velocities in the channel because of the scarcity of such data. The fluctuating motions in the waves have been investigated elsewhere and appear to be reasonably well-described by several available theories and numerical models. The exceptions occur in and near the breaking region of the wave where measurements of any sort are difficult, so that poor comparisons may not be a failure of the theory. The wave-induced mean velocities are small and often are contained within much larger fluctuating motions over a major portion of water column. Therefore we elected to measure the mean motions via the movement of a slightly buoyant tracer particle. A multiple exposure photograph of a rising polystyrene bead in waves is shown in Figure 3. Similar photographs were taken several times during a test run, always in the same location along the convergent channel (x = 27 ft or 8.2m). The bead motion near the surface was generally lost in the multiple exposures of the instantaneous free surface. In the future the procedure could be improved by shading the camera from this region until just before the bead enters.

The sequence of bead locations together with several reference locations from the background grid (white lines) and the near wall (black crosses) were digitized using a graphics tablet interfaced to a small desk-top computer. The perspective of the photographs was determined and the bead positions were calibrated as shown, for example, by the data in Figure 4 which corresponds to the photograph in Figure 3. The bead was assumed to remain in the midplane of the channel after a number of preliminary tests indicated this to be a reasonable assumption. It would not be very difficult to add a stereoscopic view for wave flows that contain significant transverse motions. The digitization process also could be readily automated using digital video techniques.

The mean velocity in the channel was assumed to have two contributions: a wave transport U_* to the right which decayed exponentially with depth and a uniform return flow $\bar{U}$ which gave a net mass transport of zero at any location along the channel. These mean motions could be removed from the data to yield the wave-induced velocities, but this effort was discontinued in view of the lack of near surface data and preliminary comparisons with theory as shown by the solid line in Figure 4. There the linear wave theory compares well with the data when it is corrected to include the mass transport, the buoyancy of the bead and the measured return flow in the channel. Differences which existed between the linear theory and higher-order theories at these depths were well within the accuracy of the data, since the velocities were found from differences between data points (position) and therefore the velocity results were prone to be more scattered.

2.4 Visual Records of Wave Breaking Still photographs of the instantaneous wave profile in the uniform test section were taken to identify features of the breaking process which might escape detection by the wave height probes. A typical photograph is shown in Figure 5. The wave is illuminated from below using a standard fluorescent lighting tube. The tube became imaged in the meniscus at the wall of the flume and in the free surface of the wave. The horizontal white line in the photograph is the meniscus of

the still water behind the uniform test section and serves as a reference for the measurements since the entire wavelength was not always captured in the photograph. The contrast in these photographs was adequate for digitization using a video system. The wave profile and the dimensions of the 'white-water' region were retained to yield local slopes and overall features of the breaking region. This technique could be refined in the future to yield details of the breaking region such as local void fractions and entrained bubble or white water characteristics. Most of the required improvements are in the methods of illumination and could be obtained through the use of narrow sheets of light and possibly certain dyes as done by Duncan (1981, 1983).

During the final experiments a video camera set to one side of the work area recorded the overall wave pattern in the channel at the time. This provided a permanent visual record of intermittent breaking events to augment the data acquisition sequence from the wave probes. In this way we could permanently catalog various locations and types of breaking in conjunction with the recorded wave heights which do not always readily distinguish between breaking and non-breaking waves or between the various types of breakers. This is a common problem with conventional wave probes and it stems from limitations in amplitude resolution and frequency response. The best solution to these difficulties may be to utilize optical methods to obtain all of the wave breaking data. Video devices which can accomplish this are becoming available.

3. EXPERIMENTAL RESULTS AND DISCUSSION

3.1 Steep, Non-breaking Wave Characteristics The first and simplest comparison between the observed and predicted nonlinear wave characteristics is shown in Figure 6 where the ratio of the measured phase speed to the linear theory prediction is plotted versus the measured wave steepness H/L_*. The measured phase speeds shown in the figure were determined simply from the time required for an individual crest to travel between the two

wave probes. This was plotted versus the steepness at the midpoint between the probes. The third-order Stokes prediction is shown in the figure as the solid line while the dashed line represents the apparent third-order phase speed as if it were determined in the same manner as the experiment, i.e. averaged over the same growth interval and plotted at the midpoint wave steepness. The overall agreement is good. The scatter, particularly at low values of steepness, is mostly due to the cross waves in the channel which can introduce significant timing errors for the local wave elevation maximum. The general agreement with the third-order phase speed carries the requirement for similar agreement with the third-order wavelength.

A typical plot of a very steep, symmetrical wave profile is shown in Figure 7a. There is good agreement between the experiments and the third-order theory. Our data is a time series for a fixed location, but Van Dorn and Pazan (1975) have shown that for the growth rates of their study and of the present study a simple space-time equality is valid within experimental accuracy. Figures 7b and 7c show asymmetric wave profiles which are representative of several runs where waves were breaking a bit further downstream in the channel. The asymmetries, α, as measured by the ratio of one half-wavelength to the horizontal distance between the crest and the preceding trough, differ for the two profiles shown and are related to the form or type of breaking observed. This is discussed later in the section on breaking waves. The asymmetries of the waves will, of course, preclude any agreement with predicted profiles from Stokes expansions of any order because the latter are all symmetric. Within the accuracy of our results ($\pm 3\%$) the phase speeds and wavelengths of steep, asymmetric waves continued to be well-represented by third-order predictions. This observation is somewhat paradoxical because the asymmetry must develop from a crest "over taking" the trough ahead in some way, yet our measurements do not indicate a significantly higher crest speed in these instances.

The asymmetries observed in the experiments did tend to increase slightly along the channel for a particular run, but they remained at comparable values for different runs even though the steepnesses were different. It was not possible, therefore, to relate the profile asymmetry

to the wave steepness in any systematic manner other than to note that the asymmetries of waves that eventually broke in the channel fell into two distinct ranges. The first range was $1.0 \leq \alpha \leq 1.1$ which led to spilling breakers, while the second range was $1.15 \leq \alpha \leq 1.25$ which led to curling or mildly plunging breakers. The two types of breaking are illustrated in Figure 12.

At low growth rates the waves in the channel exhibited a temporal modulation at periods near four times the wave period. In runs that produced breakers at these growth rates, the breaking event became modulated such that almost every fourth wave broke. Sometimes there were as few as two or as many as four non-breaking waves between breakers. The location of breaking also varied somewhat along the channel. The mechanism at work here is assumed to be the subharmonic instability described in Section 1.1 and which is the subject of much recent study for the case of uniform steep waves. The frequencies of all measurable subharmonic disturbances fell in the narrow range of 0.22 to 0.28 times the fundamental wave frequency. The amplitude of the subharmonics reached nearly ten percent of the wave height just prior to breaking. These results can be compared to observations of wave instabilities in initially uniform, steep wave trains as shown in Figure 8, which is adapted from Melville (1982). The curves plotted there are predictions of the dominant subharmonic frequency versus the initial steepness $ak \simeq \pi (H/L)$ from several stability analyses. The solid circles are the measurements of Melville, which are in best agreement with the prediction by Longuet-Higgins (1978b) shown by the solid line. The difficulty in comparing the present results to the uniform wave train results is the inability to prescribe an appropriate initial steepness for our data when, in fact, the steepness is forced to grow steadily by the channel convergence. We have plotted the present observations at two values of steepness corresponding to the conditions at the inlet and the outlet of the convergent section. This is somewhat arbitrary and is done to bracket the range of possible choices. Assuming that the appropriate value of steepness is somewhere in the middle of the bracketing values, the present

results are comparable to Melville's observations and to the various theories plotted in the figure.

The comparison with instability theory is pursued further in Figure 9, which is adapted from Longuet-Higgins (1978b), where the unstable region is shown in the plane of the modulation frequency versus the initial wave steepness. According to this figure and to the analogy that we are pursuing, the waves in the channel also ought to have exhibited unstable modes at one-fifth and less of the wave frequency. This was not observed in the present experiments and the simple analogy fails. The instability analysis does predict that the most unstable modes overall, as determined by initial growth rates, are in the vicinity of one fourth of the wave frequency. Evidently, these modes quickly dominate in the convergent channel because of their inherent growth rates and the further growth imposed by the channel.

The wave-induced mean drift averaged over the water depth for steep, non-breaking waves was determined from Eq. (1.3.1). The results are plotted in Figure 10 versus the depth-averaged, second-order Stokes prediction, $\bar{U}_p$, which is correct to third order and is given by

$$\bar{U}_p = \pi^2 C \int_{-\infty}^{0} (H/L)^2 e^{2kz} dz, \qquad (3.1.1)$$

where z is measured positive upward from the mean position of the free surface. The solid line in the figure represents $\bar{U} = \bar{U}_p$ and indicates that the total mass transport is satisfactorily predicted by the Stokes'second-order theory (correct to third order).

The phase speed and the return drift current in the channel were used together with the conservation relation given by Equation (1.3.6) to compare the observed wave growth rates with both the simple and the full conservation requirements. The total energy was assumed to be equipartitioned into kinetic and potential contributions with the potential energy given by

$$PE = \frac{1}{4} \rho g (H/2)^2 \equiv E/2. \qquad (3.1.2)$$

The errors contained in these assumptions are small and are considered within the accuracy of the measured variables. A detailed analysis of the question of energy partition was done by Van Dorn and Pazan (1975). Moreover, by primarily considering ratios of energy, the errors become less significant in any case.

If the energy is simply conserved, the total amplification ought to be the square root of the ratio of the channel widths at the two locations, which in our facility is $\sqrt{6} = 2.45$. As mentioned earlier and is evident in Figure 2, the actual growth is less than simple conservation suggests and is adequately described by Equation (1.3.6).

3.2 Criteria for Wave Breaking The limiting values of steepness H/L_* at the observed onset of wave breaking are plotted in Figure 11 as a function of the simple or nominal energy growth rate, $G = -\frac{L_*}{w}\frac{dw}{dx}$. As shown in the previous section, the actual wave growth rates were somewhat less due to several channel effects. The quantity G is used here to facilitate comparisons with the results of Van Dorn and Pazan, and it can be interpreted as a nondimensional rate of channel convergence in the sense that the wall slope is measured in units of fractional width change per limiting wavelength L_*. For any particular wave period G is an inversely linear function of position along the channel.

The limiting steepness was computed from the data in three ways. First, the spatially-smoothed average of eight wave cycles was used to obtain the solid circles in Figure 11. On this basis the observed limiting steepness increases slightly with G at lower overall values than were found previously by Van Dorn and Pazan as indicated in the figure. Next, the local values of the eight cycle averages were used to develop values of the limiting wave steepness. These data are given by the open circles and the bars on each point indicate the range of values obtained from the many individual runs. This calculation reduces the apparent dependence upon G by increasing the observed limiting steepnesses at the lowest values of G. Recalling that subharmonic modulations produced intermittent breaking at the lowest growth rates, the limiting steepnesses were recomputed using

individual, local values of only those waves which actually broke. The data obtained in this third way are represented by the crosses in the figure and the bars again serve to indicate the range of the data. The limiting steepnesses in these instances are increased further at the lowest values of G while the remaining data are essentially unchanged.

On the basis of the third method of calculation the onset criterion for wave breaking becomes independent of growth rate and all other test parameters. The significance of this result is that a wave will begin to break when the local steepness reaches $H/L_* = 0.11$ regardless of the growth process or processes that led to that local value of steepness. For example, the combination of spatial modulations and temporal modulations in a convergent channel produces waves whose steepnesses vary with both time and spatial location. The site of breaking therefore varies and follows the position where the local, instantaneous steepness first exceeds $H/L_* = 0.11$.

The present criterion for breaking is comparable to the maximum values found from studies of wave instabilities ($0.05 \leq H/L_* \leq 0.11$). The instability criterion for initially uniform, steep wave trains only states that waves above the threshold will eventually lead to breakers. At the point of breaking the local steepness is larger and approaches $H/L_* \simeq 0.11$ according to the observations of Melville (1982) and of Su et al (1982). Similarly, the surface waves generated behind a submerged, moving hydrofoil break near $H/L_* \simeq 0.11$ according to Duncan's (1983) observations.

In a study of the breaking of deep water waves in a uniform laboratory channel, Ochi and Tsai (1983) found that irregular waves in the range $gT^2 = 200$ to 800 cm were clustered around an average value of $H/L_* = 0.105$. The waves in the present experiments were in the range $gT^2 = 550$ to 1100. Thus the ranges of these and the present experiments overlap and yield comparable results for the wave breaking criterion expressed in terms of wave steepness. Thus, it appears that an invariant deepwater breaking criterion exists for a local value of wave steepness $H/L_* \simeq 0.11$, and it is largely independent of the means by which the wave reaches that value of steepness. The simplicity of this result should be useful in the further

development of models to predict the occurrence of wave breaking as discussed by Nath and Ramsey (1974), Ochi and Tsai (1983), or by Kjeldsen and Myrhaug (1978). It is important to note that the onset criterion applies equally well to two types of breakers, spilling and curling or lightly plunging.

3.3. Breaking Wave Characteristics Two types of breaking waves were observed in the present experiments. These have been termed spilling breakers and curling or mildly plunging breakers. Representative profiles for each type are shown in the photographs of Figure 12. As noted earlier the limiting steepness at breaking was the same for the two types of breakers. However, the ranges of wave asymmetries observed in the channel differed markedly with the type of breaker as listed below.

$1.0 < \alpha \leq 1.1$ → spilling breakers

$1.15 \leq \alpha \leq 1.25$ → curling breakers

The curling or mildly-plunging breakers were only observed at the larger growth rates, which is to say only observed for the longer wavelengths where the rate of channel convergence seen by the wave in one wavelength was greatest. Unlike the experiments of Van Dorn and Pazan, gently spilling breakers were also observed in the present case at these large rates corresponding to the curling breaker observations. The only remaining factor to account for breaker type was the observed difference in pre-breaking asymmetry. The cause of the difference in asymmetry and the corresponding difference in breaking type could not be established. We have speculated that, since most of the curling breakers occurred at or near the transition between the convergent section and the uniform section of the channel, local disturbances due to reflection and/or refraction enhanced the wave front steepness locally and triggered a different type of breaker. Whatever the cause, the effects upon energy losses due to breaking as well as air-entrainment processes are more pronounced as one would expect.

The fraction, F_b, of potential energy lost while breaking is defined as

$$F_b = \frac{PE - PE_b}{PE} = 1 - PE_b/PE \qquad (3.3.1)$$

where PE_b is the potential energy possessed by the breaking wave and PE is the energy it would have possessed if it had continued along the channel without breaking. For the present purposes the potential energy at a particular location in the channel is taken to be proportional to the square of the spatially-smoothed, eight cycle average of the observed waveheight, $\bar{H}(x)$. The fraction of energy lost then becomes

$$F_b = 1 - \left(\bar{H}_b(x)/\bar{H}(x)\right)^2 \qquad (3.3.2)$$

where $\bar{H}(x)$ is projected beyond the point of breaking by an extension of the pre-breaking growth process. Once the uniform width section of the channel is reached, the denominator in Eq. (3.3.2) becomes constant. The errors associated with this relatively simple determination of potential energy are small and the same errors occur in both the numerator and denominator. Thus the overall effect upon F_b should be negligible, especially if the ratio of waveheights is close to one.

The fractions of potential energy lost, computed in this way for all of the breaking wave test runs, are plotted in Figures 13a through 13g. The solid line in all of these graphs is representative of a 30 or 60 percent potential energy loss over the distance of one limiting wavelength L_*. In all but three runs the actual loss of potential energy is initially quite close to 30 percent. The three exceptions exhibit much larger rates of energy loss and have been identified with the occurence of curling or mildly plunging breakers (Figures 13e and 13f).

The waves do not continue indefinitely to lose energy through breaking, but they eventually cease to break and thereafter propagate as steep waves with a reduced amplitude and possibly a different frequency. Most of the data in Figures 14a to 14g were taken while the waves remained in a breaking condition so that the total energy lost could not be determined. The few instances where breaking activity ceased in the measurement interval are

easily seen by the limit of energy loss being reached and the fraction of potential energy lost becoming constant.

The initial fractions of potential energy lost to breaking measured from Figures 13 are plotted in Figure 14 versus the nominal growth rate G. Included on the figure are solid lines taken from Van Dorn and Pazan representing the "equilibrium" loss of potential energy which they found from their experiments which included both spilling and curling breakers..

A major conclusion of the study by Van Dorn and Pazan was that the energy lost in breaking was in equilibrium with the rate of channel convergence. This clearly was not the case in our experiments as can be seen, for example, from the data in Figures 2a to 2g. The waves continued to break and to lose energy in the uniform section of the channel. Moreover, the rates of energy loss shown in Figure 13 only became apparent after the channel convergence effect had been discounted.

By correcting for the effect of the channel convergence, a wave which commenced to break in the convergent section lost energy at the same rate that the wave would have experienced had it broken in the uniform section of the channel.

The wave-induced mass transport under conditions of breaking waves was obtained in the manner described earlier for steep waves and the results are also plotted in Figure 10. The somewhat surprising result is that the net mass transport of the breaking waves, as evidenced by the uniform return flow in the channel, does not differ measurably from the non-breaking waves. It is possible that the vertical structure of the return flow differed and therefore higher velocity layers near the floor or the surface went undetected. However, these possible mean flow differences cannot account for the bulk of the energy lost during the breaking process and one is led to conclude that most or all of the potential energy lost in wave breaking goes directly into the production of turbulence and into the air entrainment processes. This is a substantial fraction of the energy in the wave and is indicative of the vigorous mixing which occurs during a an individual breaking event.

4. SUMMARY AND CONCLUSIONS

The principal conclusions of the present study can be summarized as follows

- The kinematics of steep, symmetrical deep water waves are adequately described by third-order Stokes expansions (wave profiles, phase speeds, velocities, drift).

- The energy budget within a finite-length, slowly convergent channel is governed by the conservation of the quantity $w\ E\ (U+C/2)C$, which is significantly different than a prediction by the simple conservation of potential energy.

- Subharmonic wave instabilities were observed only near one-fourth of the fundamental wave frequency and then only for the lowest wave growth rates.

- Asymmetry of steep waves was not found to be a function of local wave steepness or mean growth rate.

- The type of breaker (spilling or curling) is determined by the wave asymmetry prior to breaking.

- The onset of breaking is given by the local instantaneous value of wave steepness $H/L_* \approx 0.11$, independent of growth rate and asymmetry. This is comparable to numerous recent results under varied conditions and strongly suggests the existence of an invariant criterion for deep water wave breaking.

- The initial spilling wave energy loss rate appears to be uniform and about 30 percent of the potential energy per wavelength (cycle). Curling breaker energy loss rates may be twice as large initially.

- Potential energy losses due to breaking do not appear as a significant increase in the mean drift, and therefore they must be largely dissipated in turbulence production or in air entrainment processes.

The above conclusions can all contribute to the further development and refinement of engineering and more basic physical models for the nonlinear events surrounding wave breaking in the ocean. We would be remiss if we did not also mention our conclusion that converging channel experiments, which may appear conceptually simple are, in fact, overly complex for the purposes of isolating and studying transitional events such as wave breaking.

5. ACKNOWLEDGMENTS

The authors acknowledge the support of the Naval Research Laboratory for the research program reported here. The able assistance of M. David Andrews during the preparation and execution of the experiments is also gratefully acknowledged.

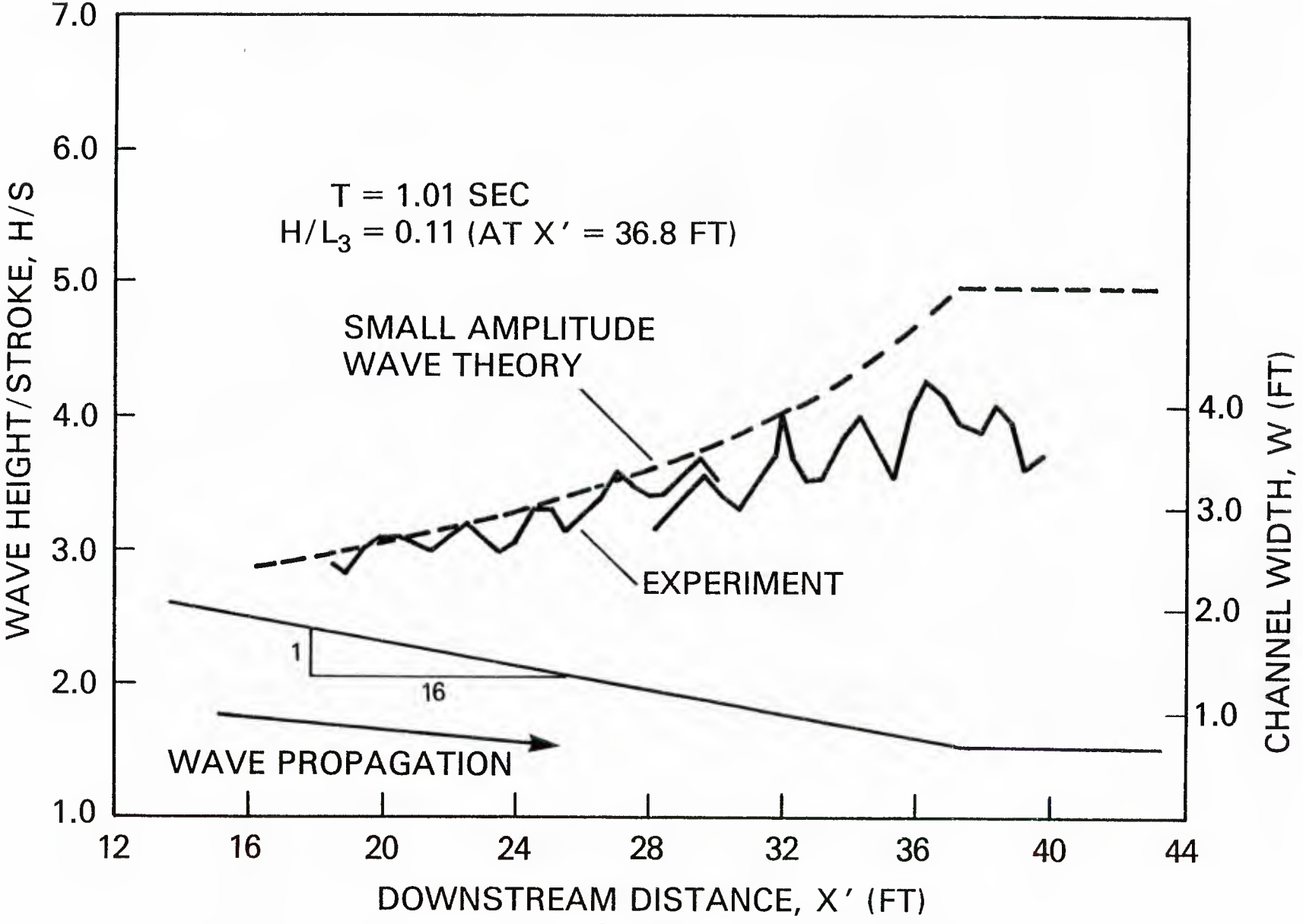

Figure 1. A schematic of the convergent wave channel together with a typical data record.

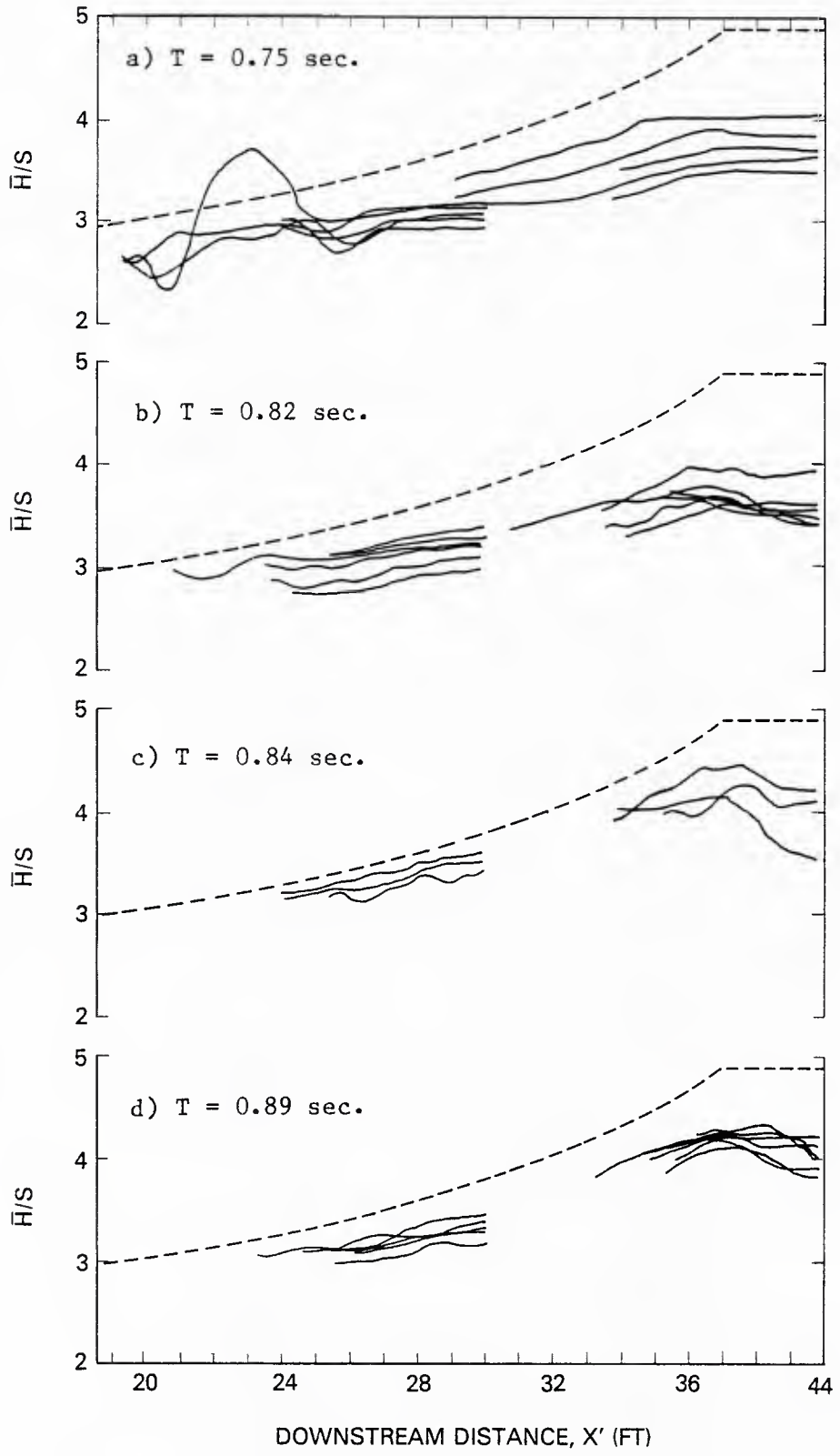

Figure 2. Averaged waveheight measured along the convergent channel.

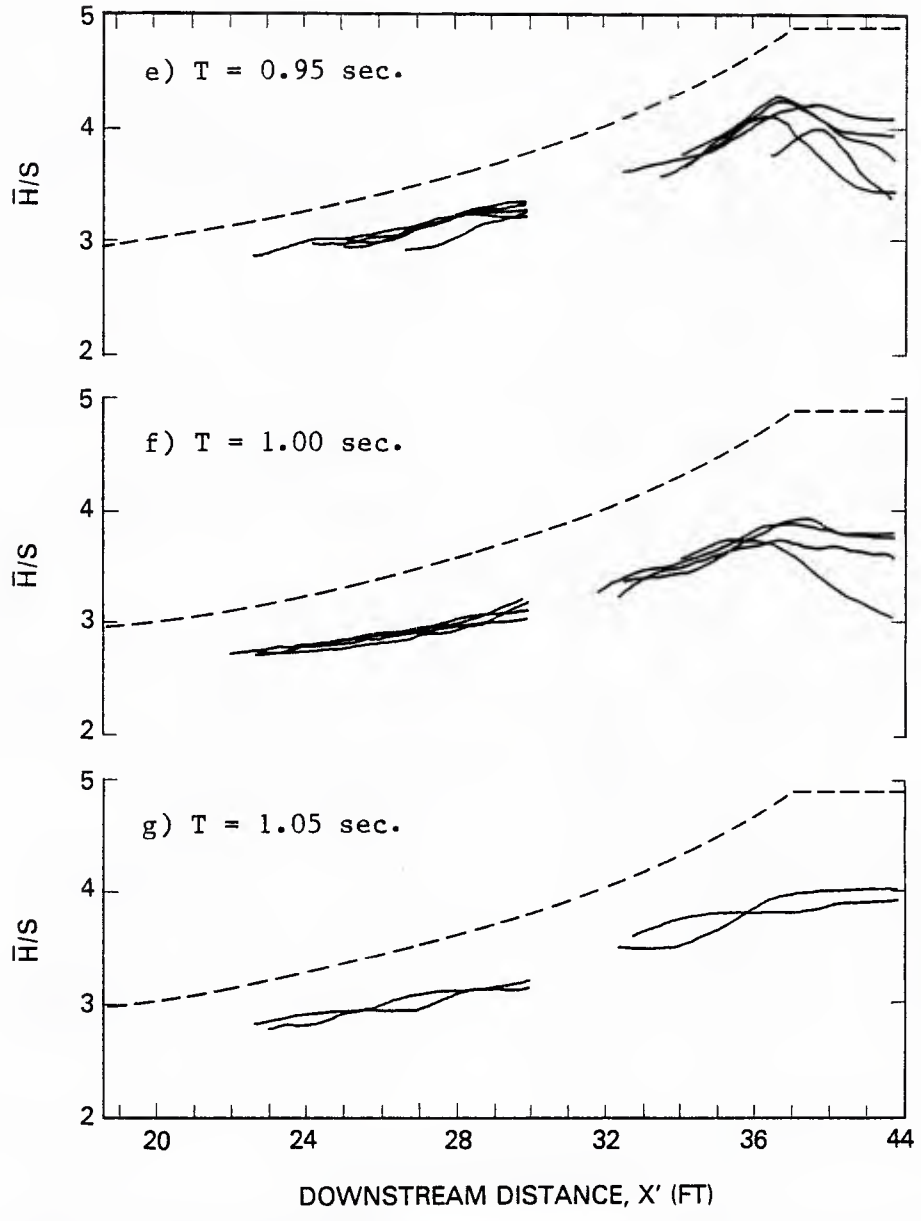

Figure 2 (Cont'd). Averaged waveheight measured along the convergent channel.

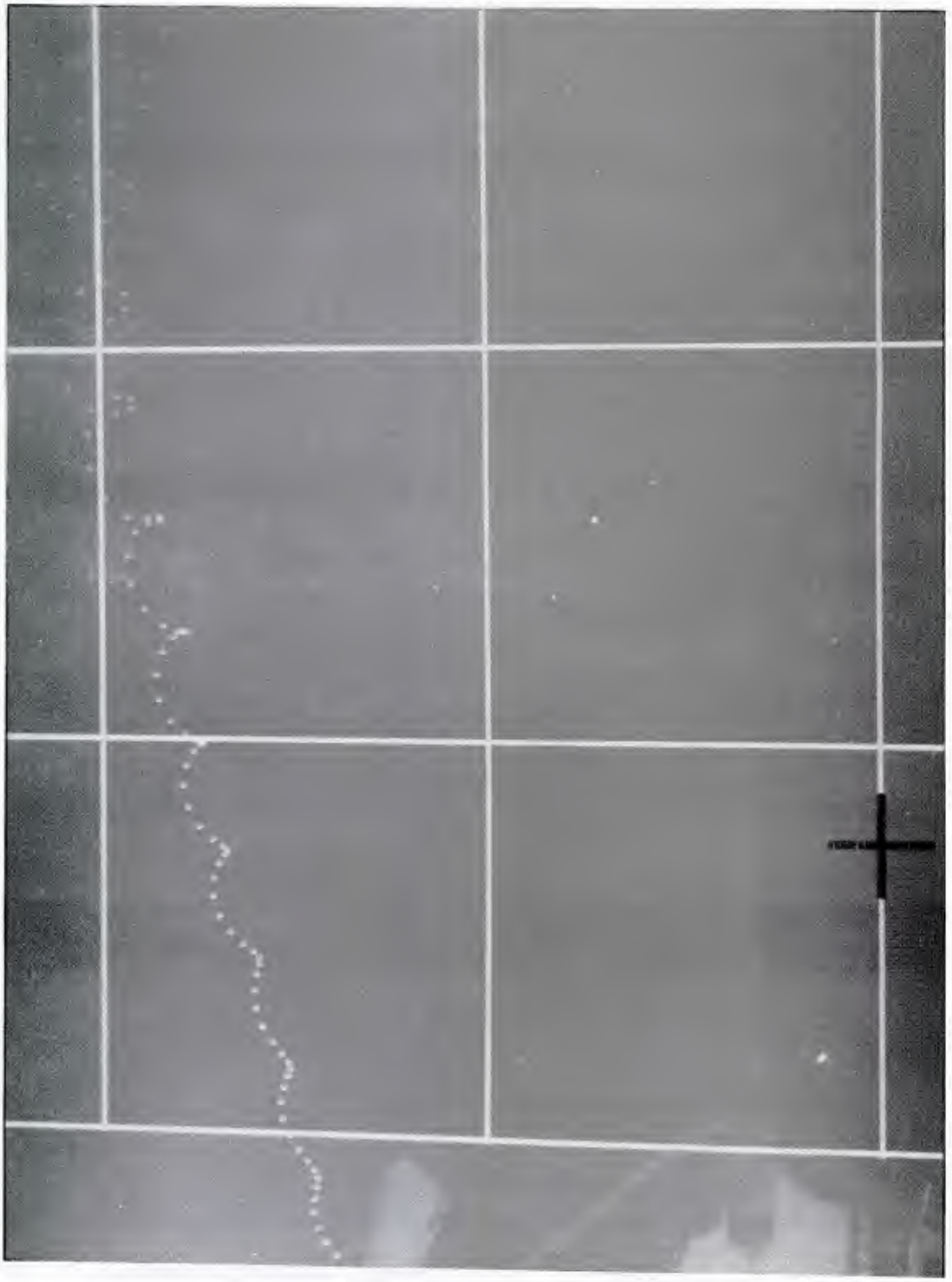

Figure 3. A multiple-exposure photograph of a rising tracer in the water column.

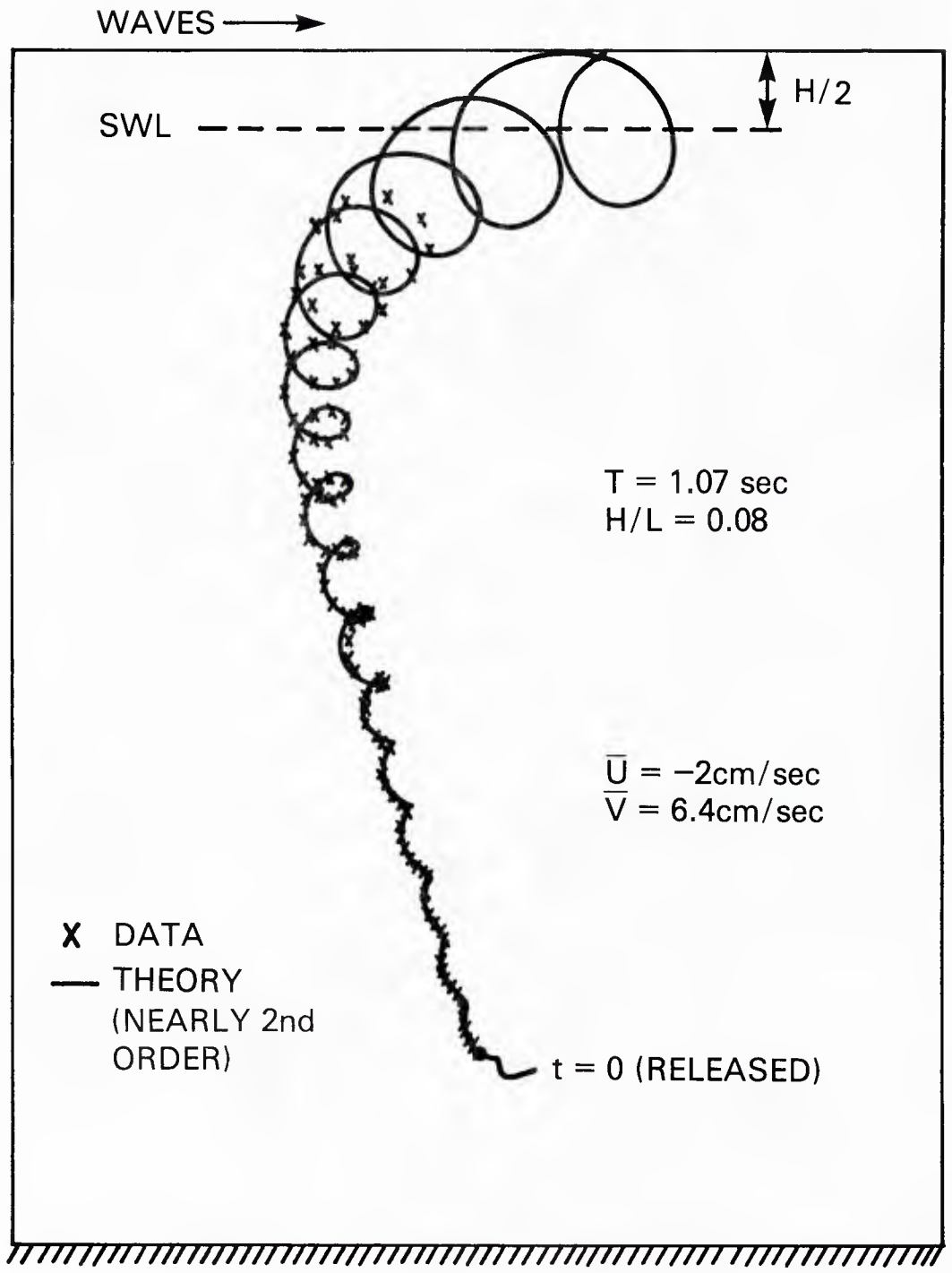

Figure 4. Calibrated bead positions from Figure 3 together with a simple prediction based upon linear wave theory with correction for wave drift and rise.

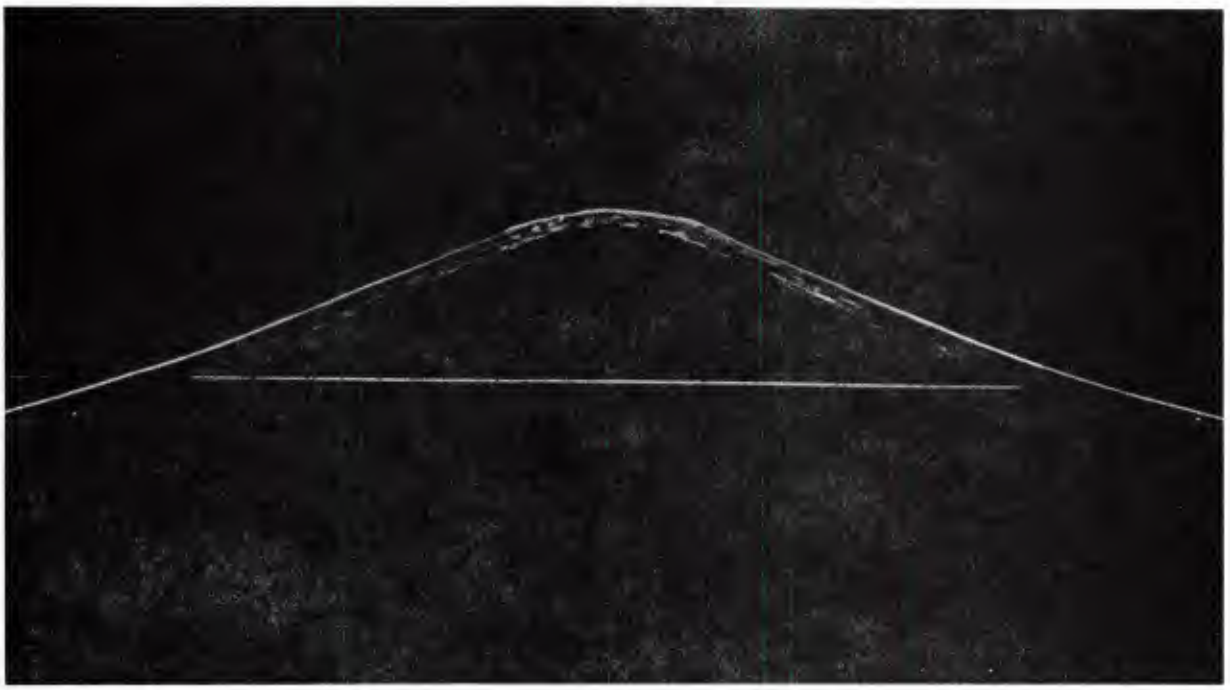

Figure 5. A photograph of the instantaneous crest profile of a steep wave.

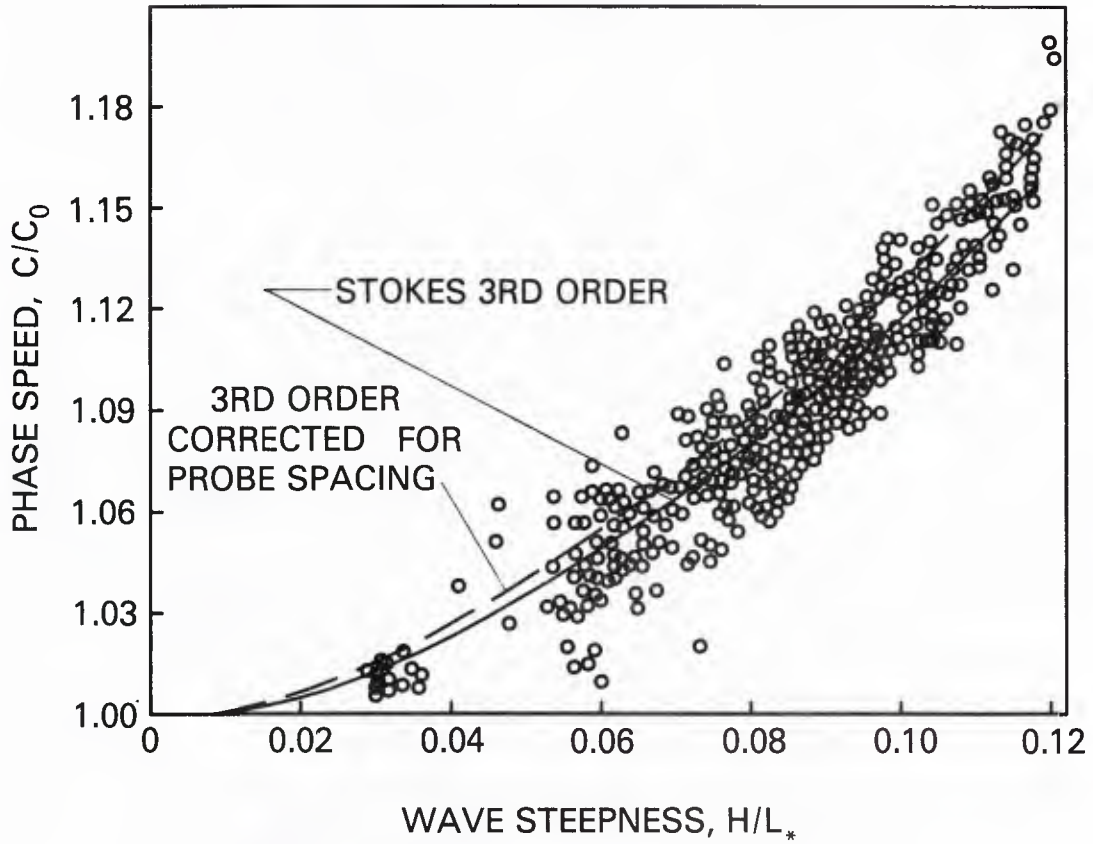

Figure 6. Phase speed versus the wave steepness.

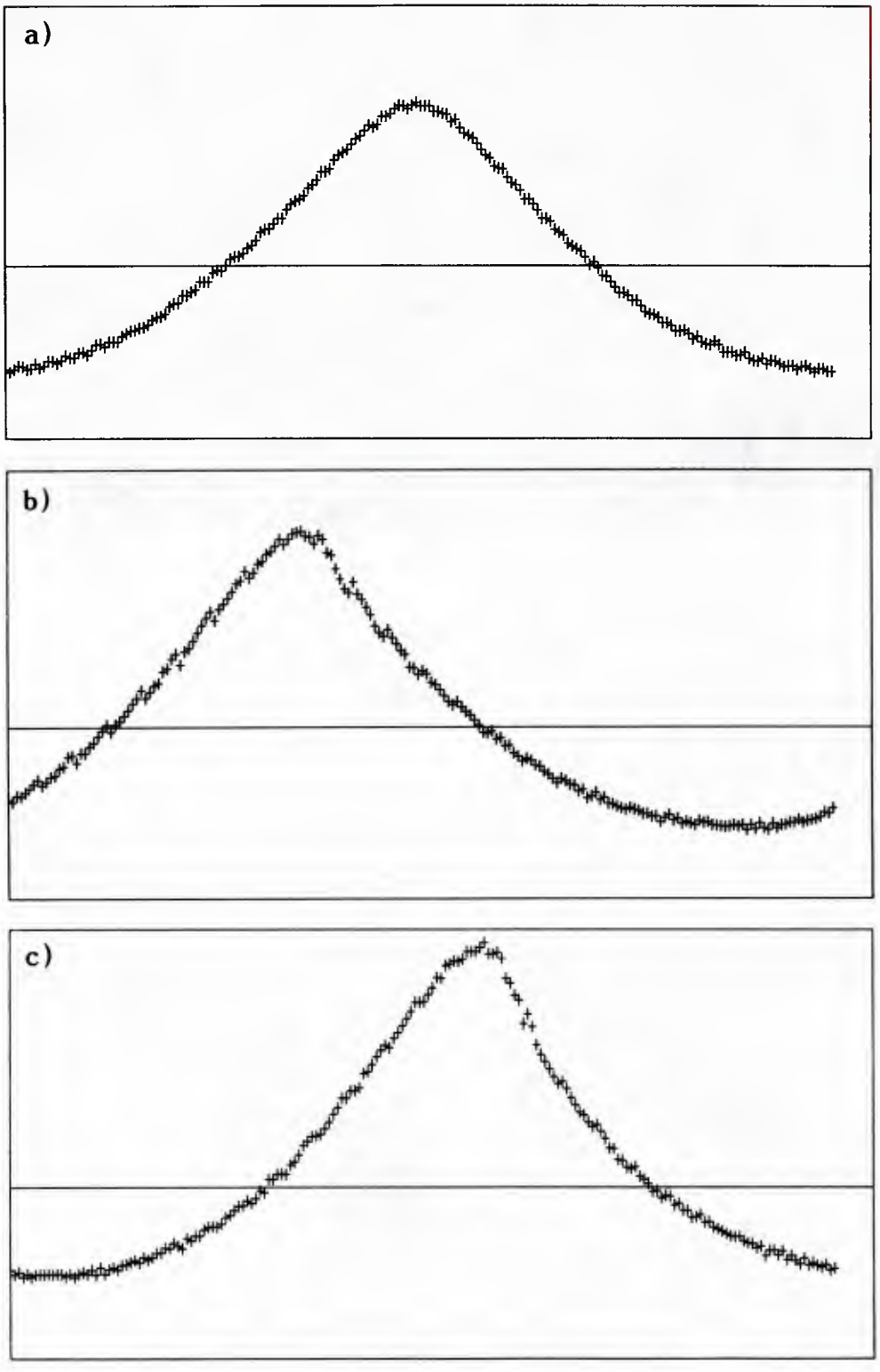

Figure 7. Measured wave profiles showing a) steep but symmetric waves, b) asymmetric waves leading to spilling breakers and c) asymmetric waves leading to curling or lightly plunging breakers.

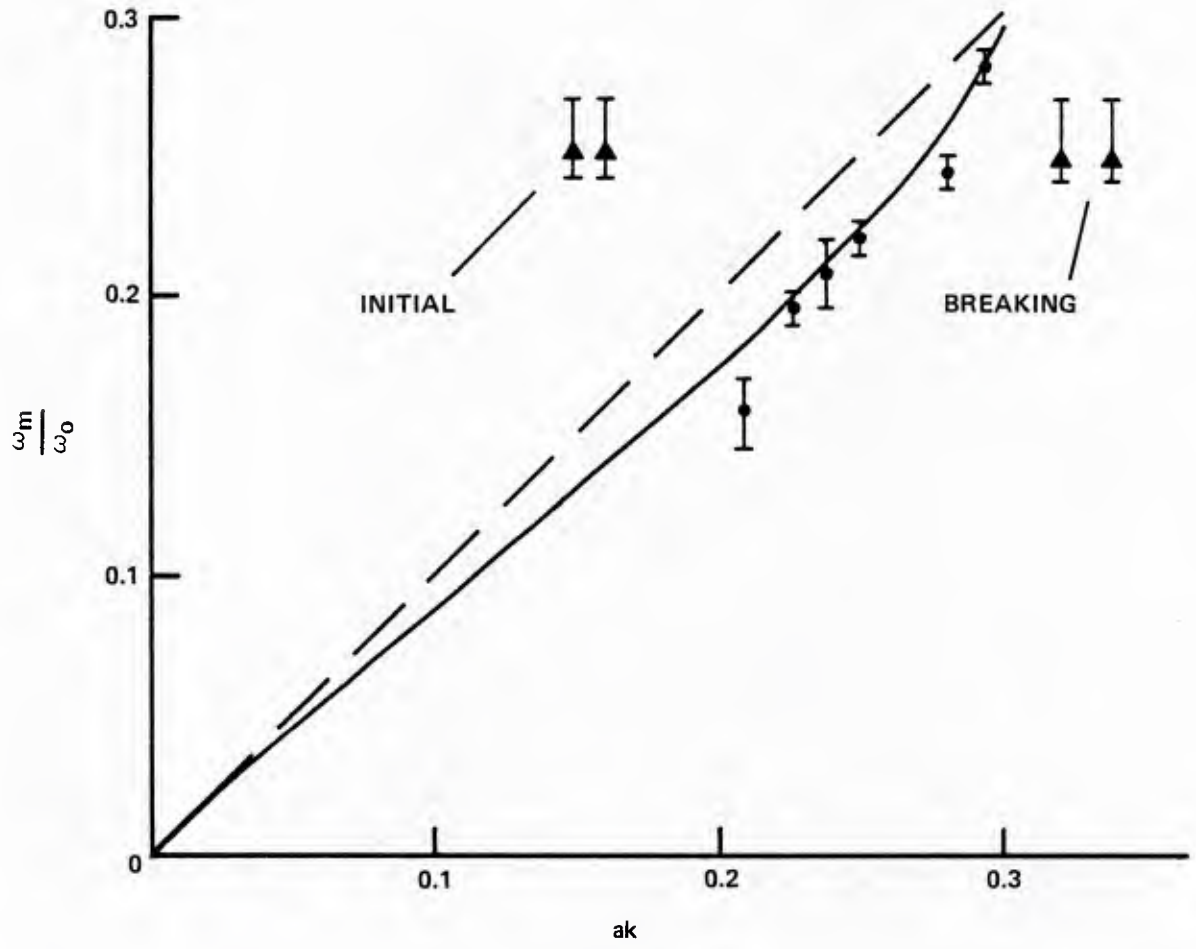

Figure 8. The frequency of the dominant subharmonic instability versus the initial wave steepness; adapted from Melville (1982). Δ, measured values, present study; ———, Longuet-Higgins (1980); — — —, Benjamin and Feir (1967).

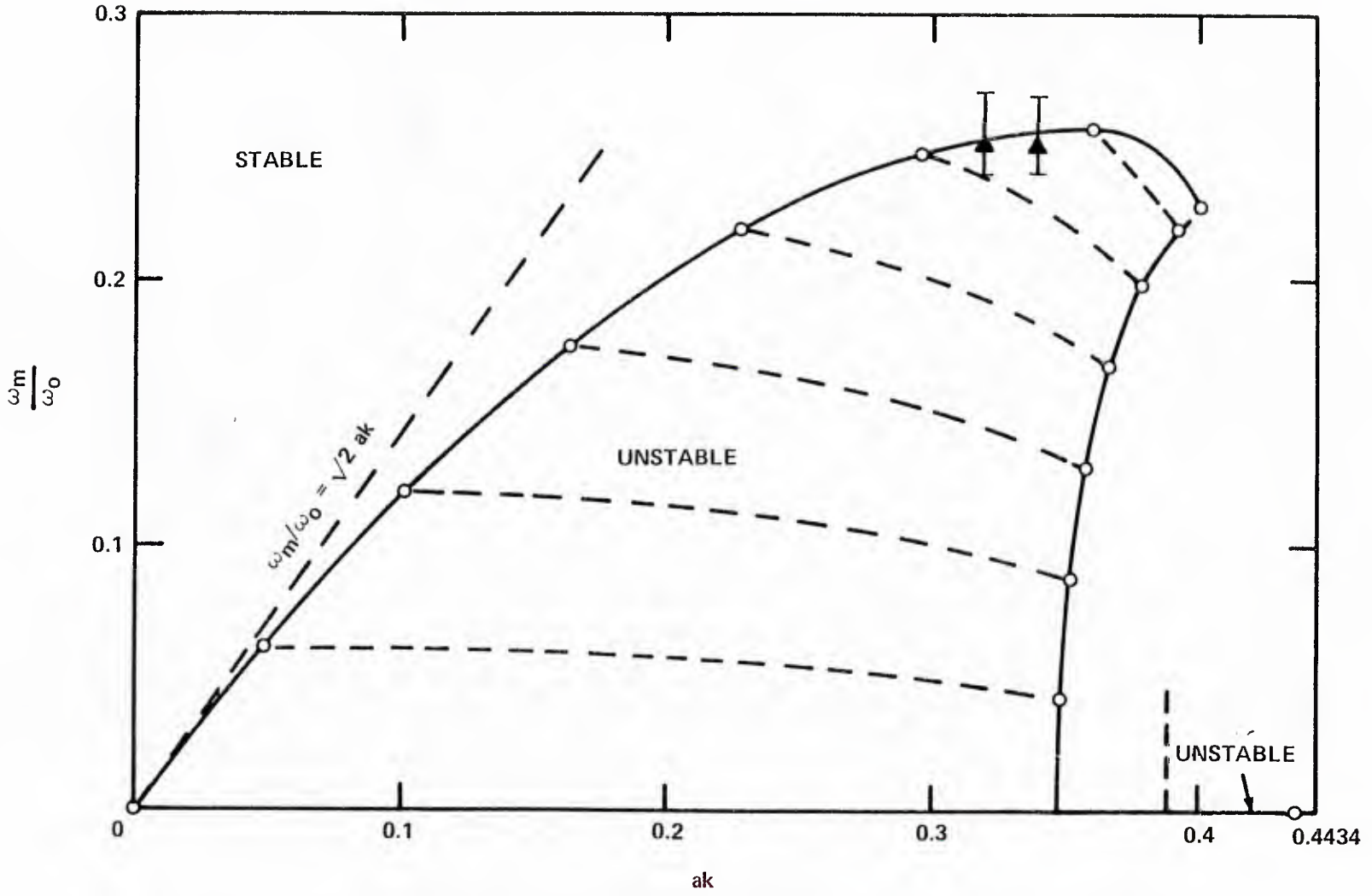

Figure 9. Instability region in the plane of subharmonic wave frequency versus the initial steepness; adapted from Longuet-Higgins (1978b). Δ, measured values, present study.

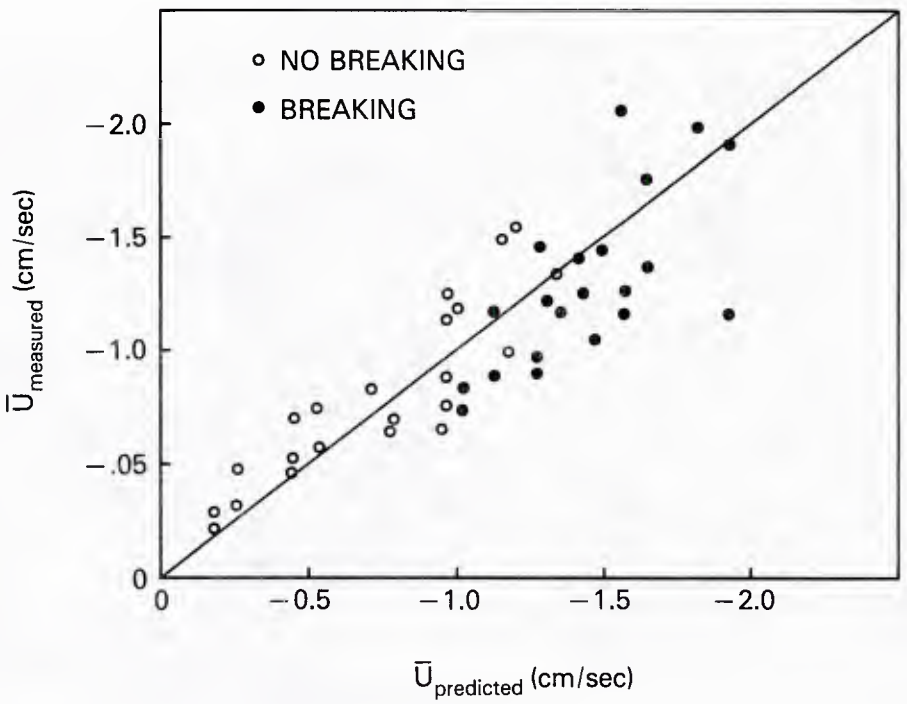

Figure 10. Measured wave-induced drift in steep waves versus the Stokes second order prediction.

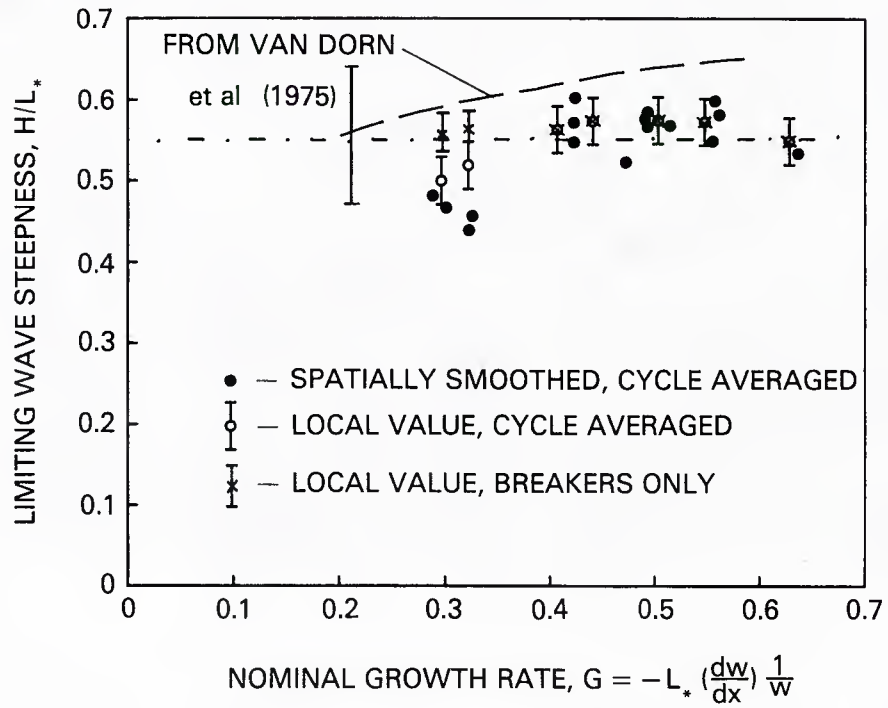

Figure 11. Limiting values of wave steepness at the onset of breaking.

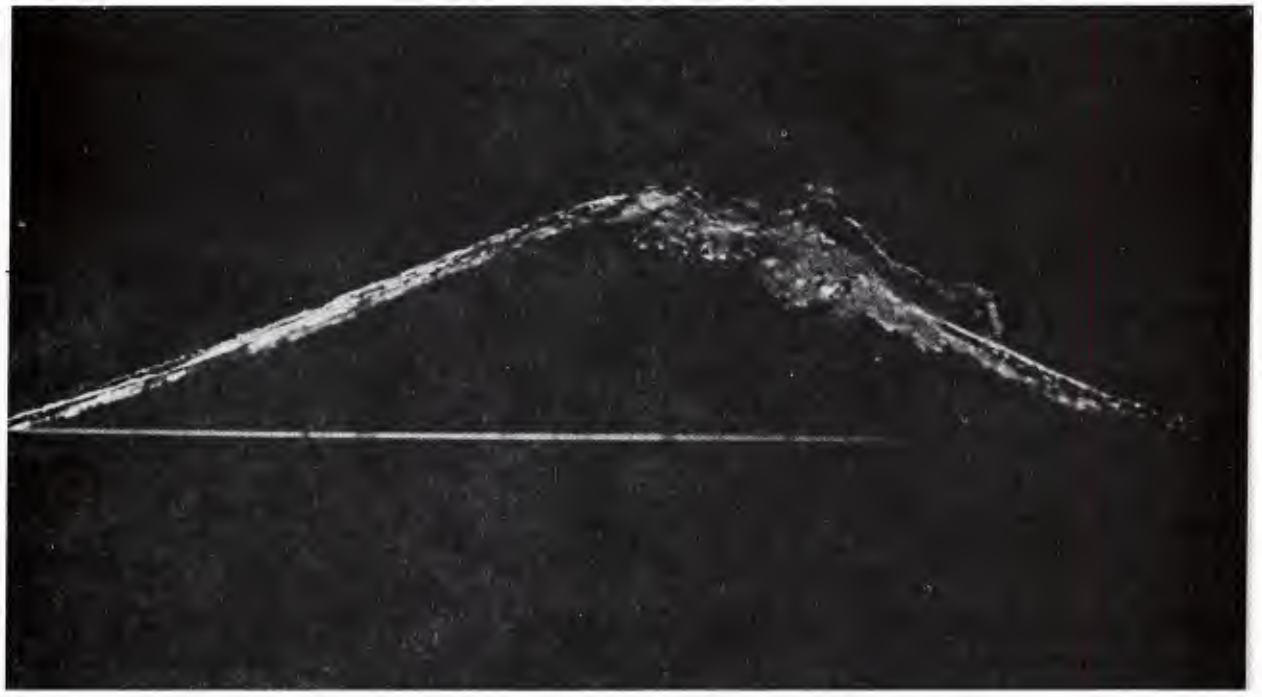

(a)

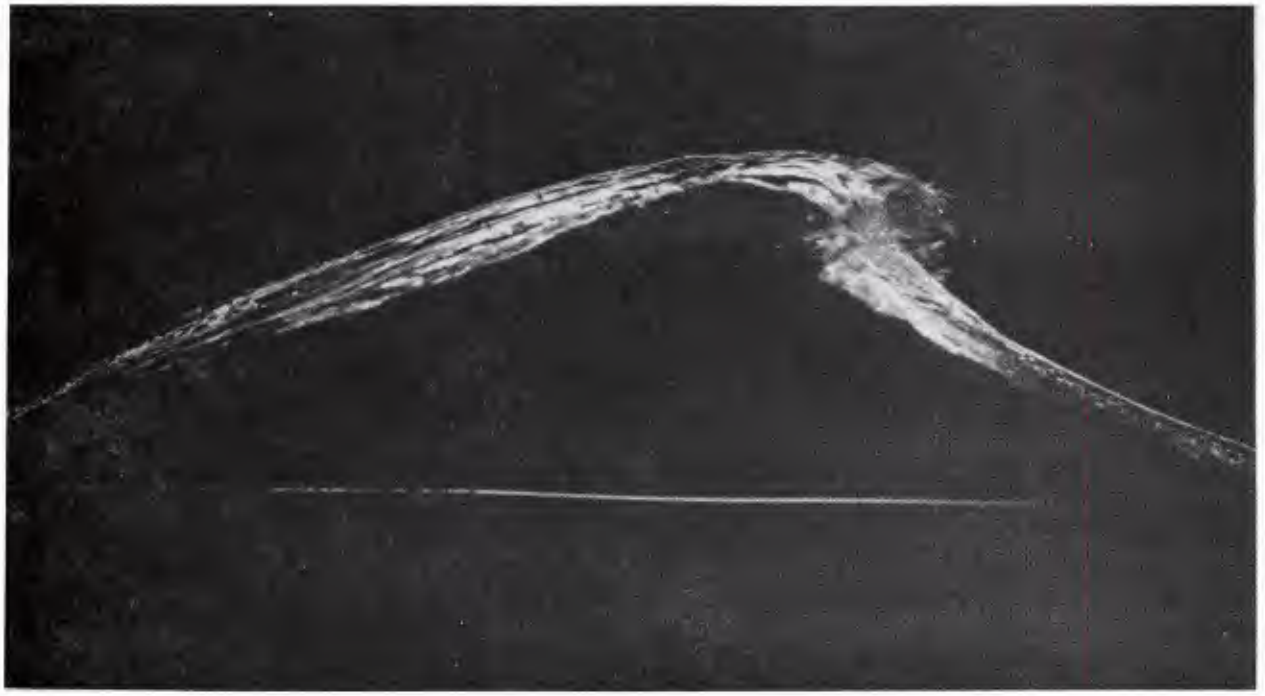

(b)

Figure 12. Typical photographs of breaking waves which were a) spilling and b) curling or lightly plunging.

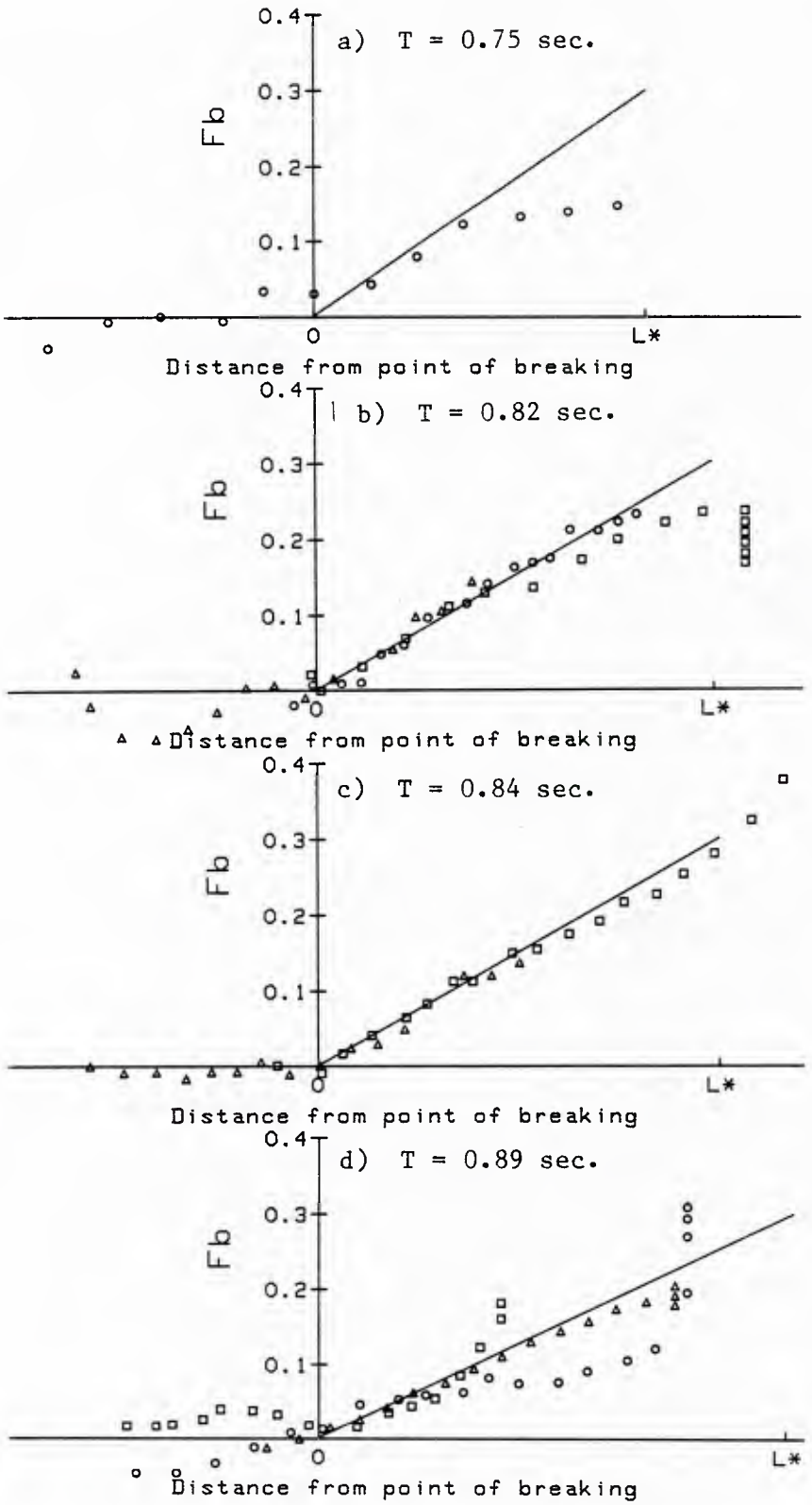

Figure 13. Fraction of potential energy lost in breaking versus the distance beyond the point of breaking inception.

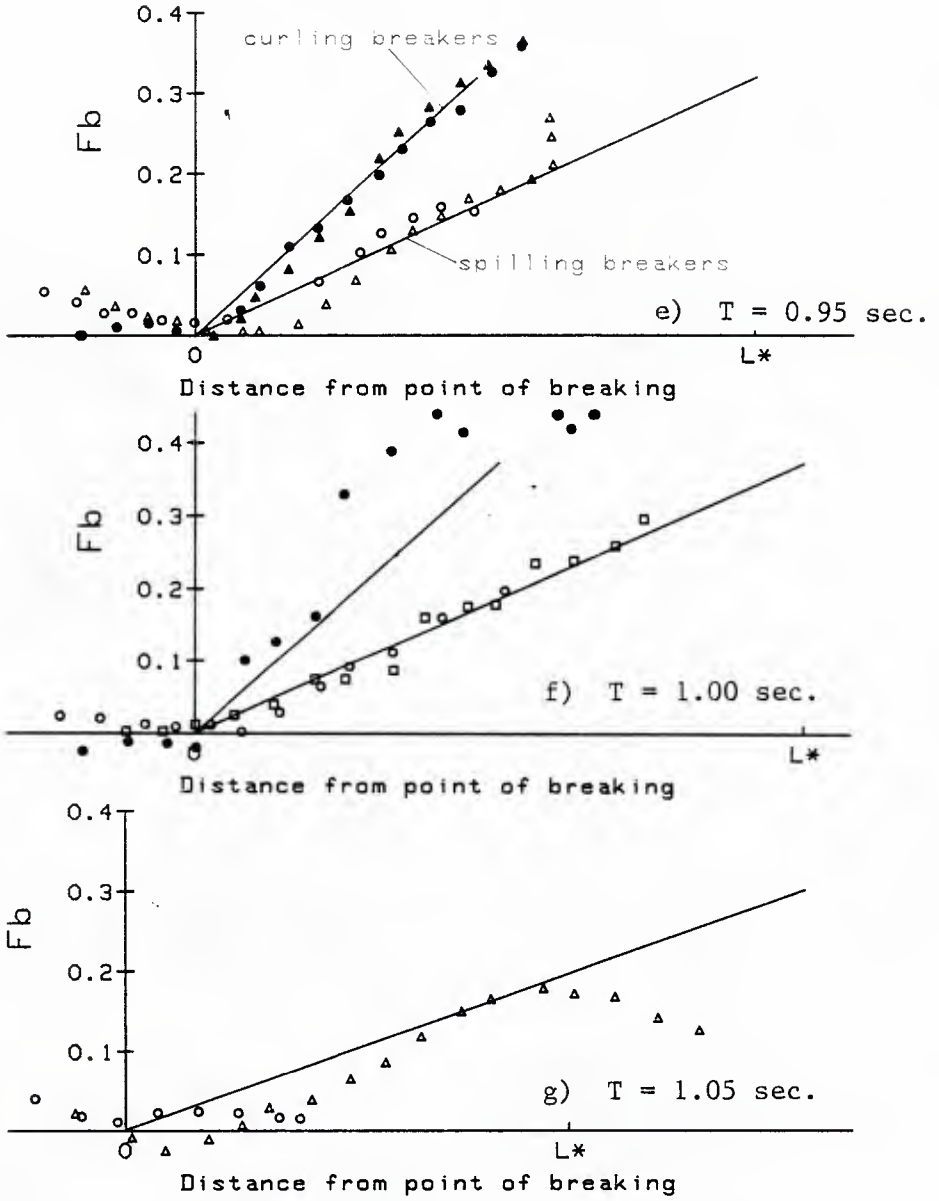

Figure 13 (Cont'd). Fraction of potential energy lost in breaking versus the distance beyond the point of breaking inception.

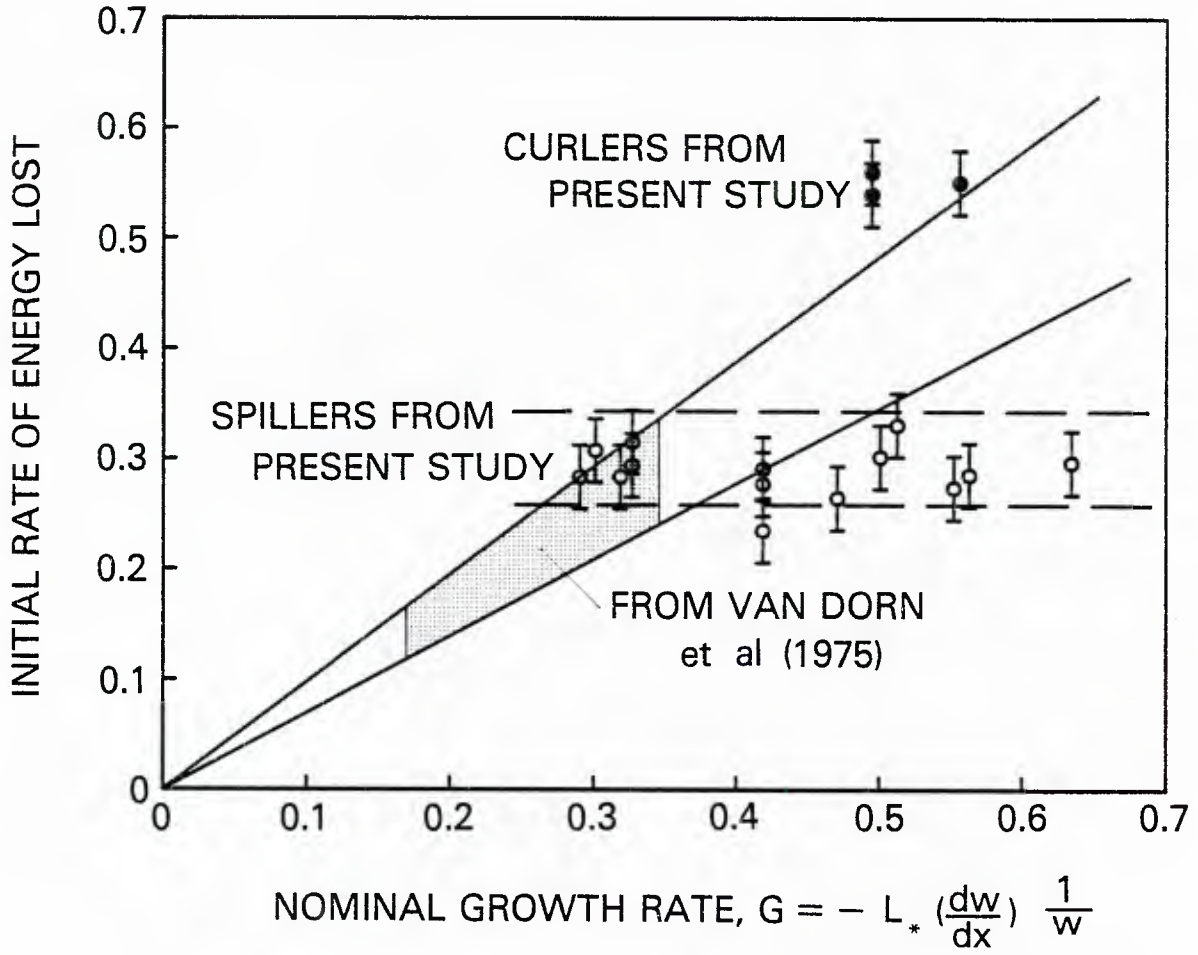

Figure 14. Initial fraction of potential energy lost to breaking versus the nominal growth rate.

6. REFERENCES

J. A. Battjes and T. Sakai, 1981, "Velocity field in a steady breaker," J. Fluid Mech., Vol. 111, 421-437.

T.B. Benjamin and J.E. Feir, 1967, "The disintegration of wave trains on deep water. Part 1: Theory," J. Fluid Mech. Vol. 27, 417-430.

E.D. Cokelet, 1977, "Breaking waves," Nature, Vol. 267, 769-774.

E.D. Cokelet, 1979, "Breaking Waves - The Plunging Jet and Interior Flow-Field," in Mechanics of Wave Induced Forces on Cylinders, T.L. Shaw (ed.), Pitman: San Francisco, 287-301.

J.H. Duncan, 1981, "An experimental investigation of breaking waves produced by a towed hydrofoil," Proc. Royal Soc. London A, Vol. 377, 331-348.

J. H. Duncan, 1983, "The breaking and non-breaking wave resistance of a two-dimensional hydrofoil," J. Fluid Mech., Vol. 126 507-520.

C.J. Galvin, Jr., 1968, "Breaker Type Classification on Three Laboratory Beaches," J. Geophys. Res., Vol. 73, No. 12, 3651-3659.

M. Greenhow, 1983, "Free-surface flows related to breaking waves," J. Fluid Mech., Vol. 134, 259-275.

O.M. Griffin and W.J. Plant, May 26, 1982, "NRL's Marine and Environmental Hydrodynamics Laboratory," NRL Memorandum Report 4786. ADA115623

O.M. Griffin, June 6, 1984, "The Breaking of Ocean Surface Waves", NRL Memorandum Report 5337. ADA142356

S.P. Kjeldsen and D. Myrhaug, 1978, "Kinematics and Dynamics of Breaking Waves," Norwegian Hydrodynamics Laboratory Report STF60A78100.

S.P. Kjeldsen and D. Myrhaug, 1979, "Breaking Waves in Deep Water and Resulting Wave Forces," Offshore Technology Conference Preprint OTC 3646.

S.P. Kjeldsen, T. Vinje and P. Brevig, 1980, "Kinematics of Deep Water Breaking Waves," Offshore Technology Conference Preprint OTC 3714.

S.P. Kjeldsen, 1979, "Shock Pressures From Deep Water Breaking Waves," in Hydrodynamics in Ocean Engineering, Norwegian Institute of Technology, 567-584.

M.S. Longuet-Higgins and E.D. Cokelet, 1976, "The deformation of steep surface waves on water. I. A numerical method of computation," Proc. Royal Soc. London A, Vol. 350, 1-26.

M.S. Longuet-Higgins and E.D. Cokelet, 1978, "The deformation of steep surface waves on water. II. Growth of normal-mode instabilities," Proc. Royal Soc. London A, Vol. 364, 1-28.

M.S. Longuet-Higgins, 1974, "Breaking Waves - in Deep or Shallow Water," Proc. Tenth Naval Hydrodynamics Symp., Office of Naval Research, 597-605. ACR204

M.S. Longuet-Higgins, 1978, "The instabilities of gravity waves of finite amplitude in deep water. I. Superharmonics, Proc. Royal Soc. London A, Vol. 360, 471-488.

M.S. Longuet-Higgins, 1978, "The instabilities of gravity waves of finite amplitude in deep water. II. Subharmonics," Proc. Royal Soc. London A, Vol. 360, 489-505.

M.S. Longuet-Higgins, 1982, "Parametric solutions for breaking waves," J. Fluid Mech., Vol. 121, 403-424.

P.A. Madsen and I.A. Svendsen, 1983, "Turbulent Bores and Hydraulic Jumps," J. Fluid Mech., Vol. 129, 1-25.

J.W. McLean, Y.C. Ma, D.U. Martin, P.G. Saffman and H.C. Yuen, 1981, "Three-dimensional in stability of finite-amplitude water waves," Phys. Rev. Lett., Vol. 46, 817-820.

P. McIver and D.H. Peregrine, 1981, "Comparison of Numerical and Analytical Results for Waves that are Starting to Break," in Hydrodynamics in Ocean Engineering, Norwegian Institute of Technology, 203-215.

W.K. Melville, 1982, "The instability and breaking of deep-water waves," J. Fluid Mech., Vol. 115, 165-185.

M. Miche, June 1954, "Undulatory movements of the sea in constant or decreasing depth. Limited form of the wave at the time of breaking. Application to Marine Structures," Univ. Cal. Inst. Engineering Res. Wave Research Lab., Series 3, Issue 363, 96 pgs.

J.H. Michell, 1893, "The Highest Waves in Water," Phil. Mag., Vol. 36, 431-437.

T. Nakagawa, 1983, "On characteristics of the water-particle velocity in a plunging breaker," J. Fluid Mech., Vol. 126, 251-268.

J.H. Nath and F.L. Ramsey, 1974, "Probability Distributions of Breaking Wave Heights," Ocean Wave Measurement and Analysis, B.L. Edge and O.T. Magoon (co-chairmen: Waves '74.), Vol. 1, 379-395, ASCE: New York.

A. L. New, 1983, "A class of elliptical free-surface flows," J. Fluid Mech., Vol. 130, 219-239.

M.K. Ochi and C.-Han Tsai, 1983, "Prediction of Occurrence of Breaking Waves in Deep Water," J. Phys. Oceanography, Vol. 13, 2008-2019.

D.H. Peregrine, 1976, "Interaction of Water Waves and Currents," in Advances in Applied Mechanics, Vol. 16, C.-S. Yih (ed.), Academic Press: New York, 9-117.

D.H. Peregrine, 1979, "Mechanics of Breaking Waves - A Review of Euromech 102," in Mechanics of Wave-Induced Forces on Cylinders, T.L. Shaw (ed.), Pitman: San Francisco, 204-214.

D.H. Peregrine and I.A. Svendsen, 1978, "Spilling breakers, bores and hydraulic jumps," Coastal Engineering 1978, ASCE; NEW YORK, 540-550.

D.H. Peregrine, E.D. Cokelet and P. McIver, 1980, "The Fluid Mechanics of Waves Approaching Breaking," Coastal Engineering 1980, ASCE: New York, 512-528.

O.M. Phillips, 1977, The Dynamics of the Upper Ocean, (2nd edition), Cambridge University Press: Cambridge, Chapter 3.9.

M.J.F. Stive, 1980, "Velocity and Pressure Fields of Spilling Breakers" Delft Hydraulics Laboratory Publication No. 233.

M.-Y. Su, M. Bergin, P. Marler and R. Myrick, 1982, "Experiments on Nonlinear Instabilities and Evolution of Steep Gravity-Wave Trains, J. Fluid Mech., Vol. 124, 45-72.

M.-Y. Su, 1982, "Three dimensional deep-water waves. Part 1. Experimental measurement of skew and symmetric wave patterns", J. Fluid Mech., Vol. 124, 73-108.

M.-Y. Su, A.W. Green and M.T. Bergin, 1984, "Experimental Studies of Surface Wave Breaking and Air Entrainment", in Gas Transfer at Water Surfaces, W. Brutsaert and G.H. Jirka (eds.), D. Reidel, 211-219.

M.-Y. Su and A.W. Green, 1984, "Coupled two- and three-dimensional instabilities of surface gravity waves", Phys. Fluids, submitted for publication.

W.G. Van Dorn and S.E. Pazan, 1975, "Laboratory Investigation of Wave Breaking. Part II: Deep Water Waves," Scripps Institution of Oceanography Report 75-21, AD A013 336.

T. Vinje and P. Brevig, 1980, "Numerical Simulation of Breaking Waves," in Finite Elements in Water Resources, S.Y. Wang et al (eds.) University of Mississippi, 5.196-5.210.

T. Vinje and P. Brevig, 1981, "Breaking Waves on Water of Finite Depth: A Numerical Study," Ship Research Institute of Norway Report R-111.81.

T. Vinje and P. Brevig, 1981, "Numerical simulation of breaking waves," Adv. Water Resources, Vol. 4, 77-82.

Appendix - Experimental Conditions

First series, T = 0.75 sec.
Bulkhead wave maker strokes (cm) = 2.10, 2.62, 2.64

Second series, T = 0.82 sec.
Bulkhead wavemaker strokes (cm) = 1.34, 2.39, 2.95, 3.45

Third series, T = 0.84 sec.
Bulkhead wavemaker strokes (cm) = 3.08, 3.45, 3.99

Fourth series, T = 089 sec.
Bulkhead wavemaker Strokes (cm) = 3.22, 3.40, 3.64, 3.89, 4.28

Fifth series, T = 0.95 sec.
Bulkhead wavemaker strokes (cm) = 4.19, 4.52, 4.82

Sixth series, T = 1.00 sec.
Bulkhead wavemaker strokes (cm) = 4.77, 5.23, 5.89

Seventh series, T = 1.05 sec.
Bulkhead wavemaker strokes (cm) = 5.29, 5.60

DEPARTMENT OF THE NAVY

NAVAL RESEARCH LABORATORY
Washington, D.C. 20375-5000

OFFICIAL BUSINESS
PENALTY FOR PRIVATE USE, $300

POSTAGE AND FEES PAID
DEPARTMENT OF THE NAVY
DoD-316
THIRD CLASS MAIL